Lithos 300–301 (2018) 121–135

Contents lists available at ScienceDirect

Lithos

journal homepage: www.elsevier.com/locate/lithos

A middle Permian ophiolite fragment in Late Triassic greenschist- to blueschist-facies rocks in NW Turkey: An earlier pulse of suprasubduction-zone ophiolite formation in the Tethyan belt

Gültekin Topuz [a,*], Aral I. Okay [a,b], Winfried H. Schwarz [c,d], Gürsel Sunal [b], Rainer Altherr [c], Andrew R.C. Kylander-Clark [e]

[a] İstanbul Teknik Üniversitesi, Avrasya Yer Bilimleri Enstitüsü, TR34469, Maslak, Istanbul, Turkey
[b] Istanbul Teknik Üniversitesi, Maden Fakültesi, Jeoloji Mühendisliği Bölümü, TR34469, Maslak, Istanbul, Turkey
[c] Institut für Geowissenschaften, Universität Heidelberg, Im Neuenheimer Feld 234-236, 69120 Heidelberg, Germany
[d] Klaus-Tschira-Labor für Kosmochemie, Im Neuenheimer Feld 234-236, 69120 Heidelberg, Germany
[e] University of California Santa Barbara, Department of Earth Sciences, Santa Barbara, CA 93106, USA

ARTICLE INFO

Article history:
Received 5 September 2017
Accepted 5 December 2017
Available online 08 December 2017

Keywords:
Subduction initiation
Permian suprasubduction-zone ophiolite
Late Triassic accretionary complex
Tethys
Eastern Mediterranean region
Turkey

ABSTRACT

The Eastern Mediterranean region within the Tethyan belt is characterised by two main pulses of suprasubduction-zone ophiolite formation during the Early–Middle Jurassic and Late Cretaceous. Despite vast exposures of the Permo-Triassic accretionary complexes, related suprasubduction-zone ophiolites and the timing of subduction initiation leading to the formation of Permo-Triassic accretionary complexes are unknown so far. Here we report on a ~40 km long and 0.3 to 1.8 km wide metaophiolite fragment within transitional greenschist- to blueschist-facies oceanic rocks from NW Turkey. The metaophiolite fragment is made up mainly of serpentinite and minor dykes or stocks of strongly sheared metagabbro with mineral assemblages involving actinolite/winchite, chlorite, epidote, albite, titanite and phengite. The metagabbro displays (i) variable CaO and MgO contents, (ii) anomalously high Mg# (= 100 * molar MgO/(MgO + FeO_{tot})) of 75–88, and (iii) positive Eu anomalies, together with low contents of incompatible elements such as Ti, P and Zr, suggesting derivation from former plagioclase cumulates. The serpentinites comprise serpentine, ± chlorite, ± talc, ± calcite and relict Cr-Al spinel surrounded by ferrichromite to magnetite. Relict Cr-Al spinels are characterised by (i) Cr/(Cr + Al) ratios of 0.45–0.56 and Mg/(Mg + Fe^{2+}) ratio of 0.76–0.22, (ii) variable contents of ZnO and MnO, and (iii) extremely low TiO_2 contents. Zn and Mn contents are probably introduced into Cr-Al spinels during greenschist- to blueschist metamorphism. Compositional features of the serpentinite such as (i) Ca- and Al-depleted bulk compositions, (ii) concave U-shaped, chondrite-normalised rare earth element patterns (REE) with enrichment of light and heavy REEs, imply that serpentinites were probably derived from depleted peridotites which were refertilised by light rare earth element enriched melts in a suprasubduction-zone mantle wedge. U-Pb dating on igneous zircons from three metagabbro samples indicates igneous crystallisation at 262 Ma (middle Permian). Timing of the metamorphism is constrained by incremental $^{40}Ar/^{39}Ar$ dating on phengitic white mica at 201 Ma (latest Triassic). We conclude that the metaophiolite represents a fragment of middle Permian suprasubduction-zone oceanic lithosphere, involved in a latest Triassic subduction zone. These data, together with several reports in literature, indicate that the middle Permian was a time of suprasubduction-zone ophiolite formation in the Tethyan belt.

1. Introduction

Fragments of oceanic lithosphere are widespread in oceanic accretionary complexes and high-pressure/low-temperature metamorphic areas (e.g. Altherr et al., 2004; Dilek and Thy, 2006; Topuz et al., 2008; Angiboust et al., 2009; Wakabayashi, 2015, 2017). Their origins can be diverse, including (i) subducting oceanic lithosphere (e.g. Angiboust et al., 2009; Saumur et al., 2010; Wakabayashi, 2017), (ii) oceanic lithosphere overriding the subduction zone (e.g. Wakabayashi, 2017; Azer and Stern, 2007; Saumur et al., 2010), and (iii) topographic rises on the ancient ocean floor such as seamounts, oceanic plateaus and intraoceanic island arcs (e.g. Ichiyama et al., 2014; Sayit et al., 2010; Utsunomiya et al., 2011). In some cases, fragments of oceanic lithosphere are reworked during the course of accretion, wherein a variety of metamorphic, igneous and sedimentary rocks are incorporated in a serpentinite-matrix mélange (e.g. Fryer et al., 2000; Wakabayashi, 2012, 2017). The original setting of formation of the ophiolite fragments is inferred mainly from field relations, immobile elements in the basic rocks of the oceanic lithosphere and the depleted or undepleted nature

* Corresponding author.
E-mail address: topuzg@itu.edu.tr (G. Topuz).

https://doi.org/10.1016/j.lithos.2017.12.005
0024-4937/

of the mantle peridotites (e.g. Dilek and Furnes, 2011; Pearce, 2014). The combination of field relations, geochemistry and geochronology may yield significant age constraints on ancient oceanic crust, including the ages of the subducting oceanic plate and topographic rises on the ocean floor as well as formation ages of the suprasubduction-zone ophiolite.

Suprasubduction-zone ophiolites commonly form at forearc, intra-arc and back-arc settings (Dilek and Furnes, 2011; Pearce, 2003). Forearc ophiolites form at the initial stages of the subduction, whereas backarc and intra-arc ophiolites form after subduction has been established (e.g. Ishizuka et al., 2014; Pearce and Robinson, 2010; Shervais, 2001; Stern and Bloomer, 1992). In the Eastern Mediterranean region, two main pulses of the formation of suprasubduction-zone ophiolites are recognised: (i) Early to Middle Jurassic (e.g. Dilek and Thy, 2006; Rolland et al., 2009; Topuz et al., 2013a, 2013b; Çelik et al., 2013, 2016; Göncüoğlu et al., 2012), and (ii) Late Cretaceous (e.g. Çelik et al., 2006; Karaoğlan et al., 2013; Parlak and Delaloye, 1999; van Hinsbergen et al., 2016; Warren et al., 2005). Following the formation of Pangaea during the early Permian, an oceanic configuration with an easterly widening embayment resulted, extending from Greece/Turkey in the west to Indochina in the east (Fig. 1 inset) (e.g. Domeier and Torsvik, 2014; Şengör, 1984; Şengör and Atayman, 2009; Stampfli and Borel, 2002). Vestiges of the Permo-Triassic subduction in this oceanic domain are widespread in the form of accretionary complexes, especially in northern Turkey (e.g. Tekeli, 1981; Pickett and Robertson, 1996; Okay and Göncüoğlu, 2004; Robertson and Ustaömer, 2012; Topuz et al., 2004, 2014; Fig. 1). However, well-documented ophiolites related to the Permo-Triassic Tethys and timing of subduction initiation are nearly unknown.

Here we report on a large meta-ophiolite fragment, the Boğazköy meta-ophiolite, ~40 km long and 0.3–1.8 km across, from northwest Turkey which occurs in a Late Triassic accretionary complex, metamorphosed in transitional greenschist- to blueschist-facies conditions. We show that this ophiolite fragment formed in a suprasubduction-zone setting during the middle Permian (262 Ma) and was incorporated into the accretionary complex during Late Triassic subduction.

2. Geological setting and field relationships

The Sakarya zone (northern Turkey) represents a Gondwana-derived continental fragment which accreted to Laurussia (e.g. the East European Craton, Scythian Platform and Moesia) during the Early Carboniferous (Fig. 1) (Okay and Topuz, 2017). Its southern margin grew by accretion from Permo-Triassic to Late Cretaceous time with intermittent subduction erosion and accretion of intra-oceanic arcs (e.g. Okay and Nikishin, 2015; Topuz et al., 2013a, 2013b; Göçmengil et al., 2013).

The Permo-Triassic accretionary complexes, commonly subsumed under the term Karakaya Complex, cover extensive areas in northern Turkey (e.g. Okay and Göncüoğlu, 2004; Okay and Monié, 1997; Okay and Mostler, 1994; Pickett and Robertson, 1996; Robertson and Ustaömer, 2012; Tekeli, 1981; Topuz et al., 2004, 2014; Yılmaz et al., 1997; Yılmaz and Yılmaz, 2004) (Fig. 1). The Karakaya complex is

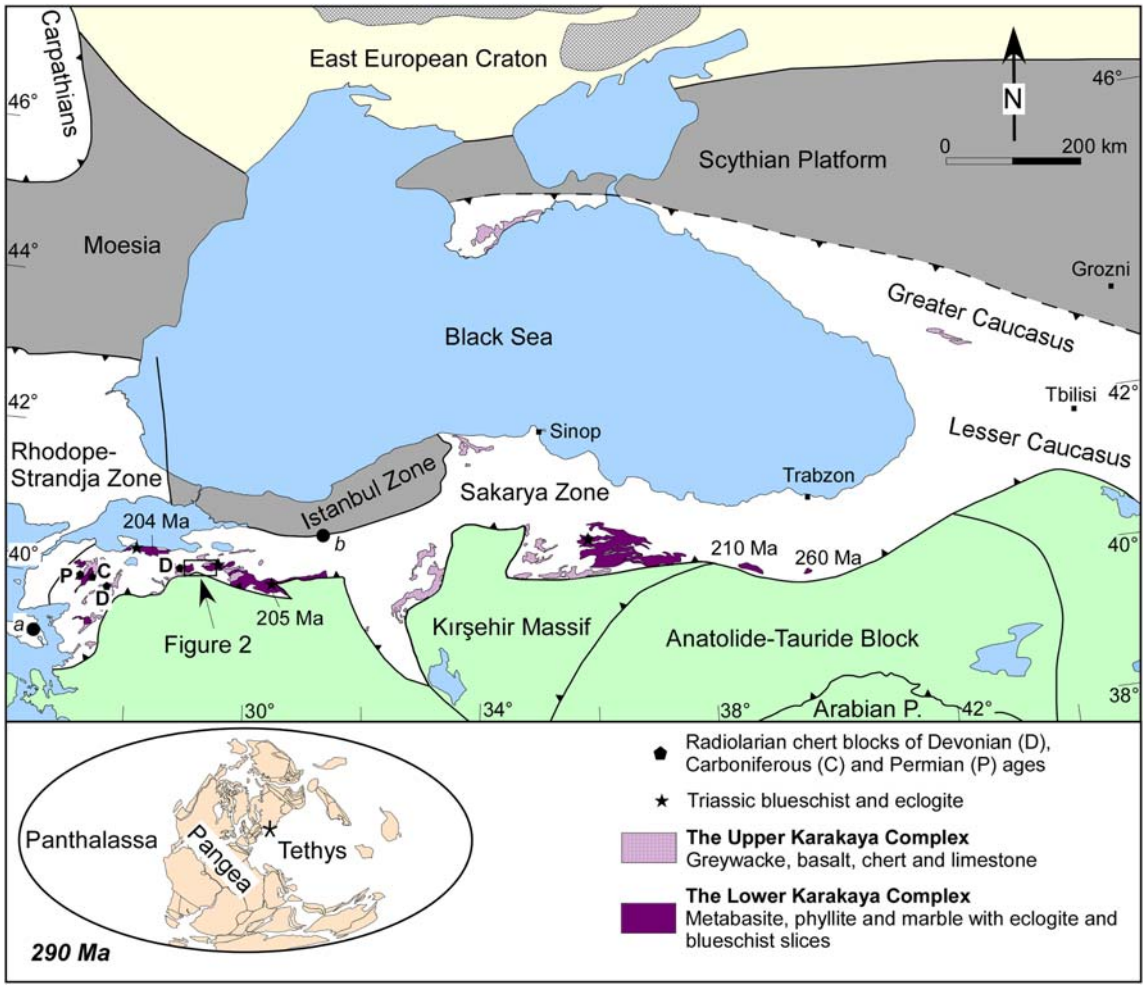

Fig. 1. Distribution of the Permo-Triassic accretionary complexes in the Sakarya Zone (modified after Okay and Nikishin, 2015; Okay and Topuz, 2017). Numbers stand for the radiometric ages of the metamorphic rocks. Filled circles stand for locations of Permian ophiolite fragments: a the Lesbos island; b the Almacık mountain. The inset shows a paleogeographic reconstruction during Early Permian (modified after Domeier and Torsvik, 2014). The star indicates the location of the Sakarya zone during the early Permian.

commonly subdivided into the Lower and Upper Karakaya complexes, separated from each other by a shear zone (Okay and Göncüoğlu, 2004; Robertson and Ustaömer, 2012). The Lower Karakaya Complex, also called the Nilüfer Unit, comprises mainly coherent rock assemblages of greenschist/blueschist- or epidote-amphibolite-facies metabasites, phyllites, marbles and minor amounts of serpentinite, metagabbro and metachert with rare tectonic lenses of eclogite (Okay et al., 2002; Okay and Monié, 1997; Topuz et al., 2004, 2014). Timing of metamorphism, constrained by $^{40}Ar/^{39}Ar$ dating on phengite, is Permo-Triassic, with ages ranging from 260 to 202 Ma (e.g. Okay et al., 2002; Okay and Monié, 1997; Topuz et al., 2004, 2014). The different age domains documented so far form isolated exposures separated by large areas of younger Mesozoic to Cenozoic cover (Fig. 1). Despite the pervasive low-grade metamorphism, the presence of Early Devonian and Permian limestone olistoliths have been documented (Çapkınoğlu and Bektaş, 1998). Sparse U-Pb zircon ages from anorogenic alkaline to tholeiitic metagabbros with a blueschist-facies overprint range from 214 to 203 Ma (Late Triassic) (Catlos et al., 2013; Eyüboğlu et al., 2011), indicating the formation of Late Triassic seamounts on the subducting oceanic lithosphere close to the trench (cf. Topuz et al., 2014).

The Upper Karakaya Complex comprises an unmetamorphosed to slightly metamorphosed tectonic pile of sheared and imbricated slices of strongly deformed sandstone, basic volcanic rock and exotic blocks of lower Carboniferous to Middle Triassic limestones and Middle Devonian to Lower Triassic radiolarian cherts (e.g. Göncüoğlu et al., 2004; Kozur and Kaya, 1994; Okay et al., 2011; Okay and Mostler, 1994). Thus, during the Permo-Triassic subduction, the age of the subducting oceanic crust ranged from at least the Middle Devonian to Early Triassic. The metabasic rocks in both the Lower and Upper Karakaya complexes dominantly display anorogenic alkaline and tholeiitic affinities similar to those in seamounts/oceanic plateaus (e.g. Genç, 2004; Okay, 2000; Pickett and Robertson, 1996; Sayit et al., 2010). The metaclastic rocks in both the Upper and Lower Karakaya complexes display similar detrital zircon age spectra characterised predominantly by Devonian, Carboniferous and Triassic ages, with the youngest ages of 207 to 227 Ma (Late Triassic) (Ustaömer et al., 2016), thus pointing to a common provenance. Relative to the Lower Karakaya complex (340 to 540 °C; 0.6 to 1.1 GPa) (e.g. Okay and Monié, 1997; Okay et al., 2002; Topuz et al., 2004, 2014; Federici et al., 2010), the Upper Karakaya complex is unmetamorphosed to slightly metamorphosed with a temperature range of 120 to 376 °C (Federici et al., 2010).

The Yenişehir metamorphic rocks (Bursa and Bilecik, NW Turkey), which constitute part of the Lower Karakaya complex form two isolated outcrops (~14 km by ~13 km and ~7 km by ~45 km), separated by the Uludağ Massif (Fig. 2). The NW-SE trending Uludağ Massif is made up of pre-Eocene amphibolite-facies gneiss, marble and amphibolite, intruded by Late Eocene-Early Oligocene two-mica granites (Okay et al., 2008; Topuz and Okay, 2017). The northeastern contact of the Uludağ Massif is represented by a normal fault, and the southeastern contact by an active transtensional fault. The Yenişehir metamorphic rocks north of the Uludağ Massif comprise transitional greenschist- to blueschist-facies metabasite, phyllite, marble, calc-schist and minor metachert (Genç, 1993; Genç and Yılmaz, 1995). To the south and southwest, the Yenişehir metamorphic rocks are locally in tectonic contact with the Upper Karakaya complex (Fig. 2). Both the Yenişehir metamorphic rocks and the Upper Karakaya complex are unconformably overlain by Lower Jurassic conglomerates and sandstones. The metabasites are characterised by anorogenic tholeiitic to alkaline within-plate affinities (Genç, 2004), and display either greenschist- or blueschist-facies mineral assemblages. Blue amphibole is more common in calcite-bearing metabasites. There is no noticeable change in the mineral assemblages towards the contact with the Boğazköy metaophiolite.

The Boğazköy meta-ophiolite forms a tectonic sliver, ~37 km long and 0.3–1.8 km wide, within the Yenişehir metamorphic rocks (Figs. 2 and 3). Strike and dip of the foliation in both the Yenişehir metamorphic

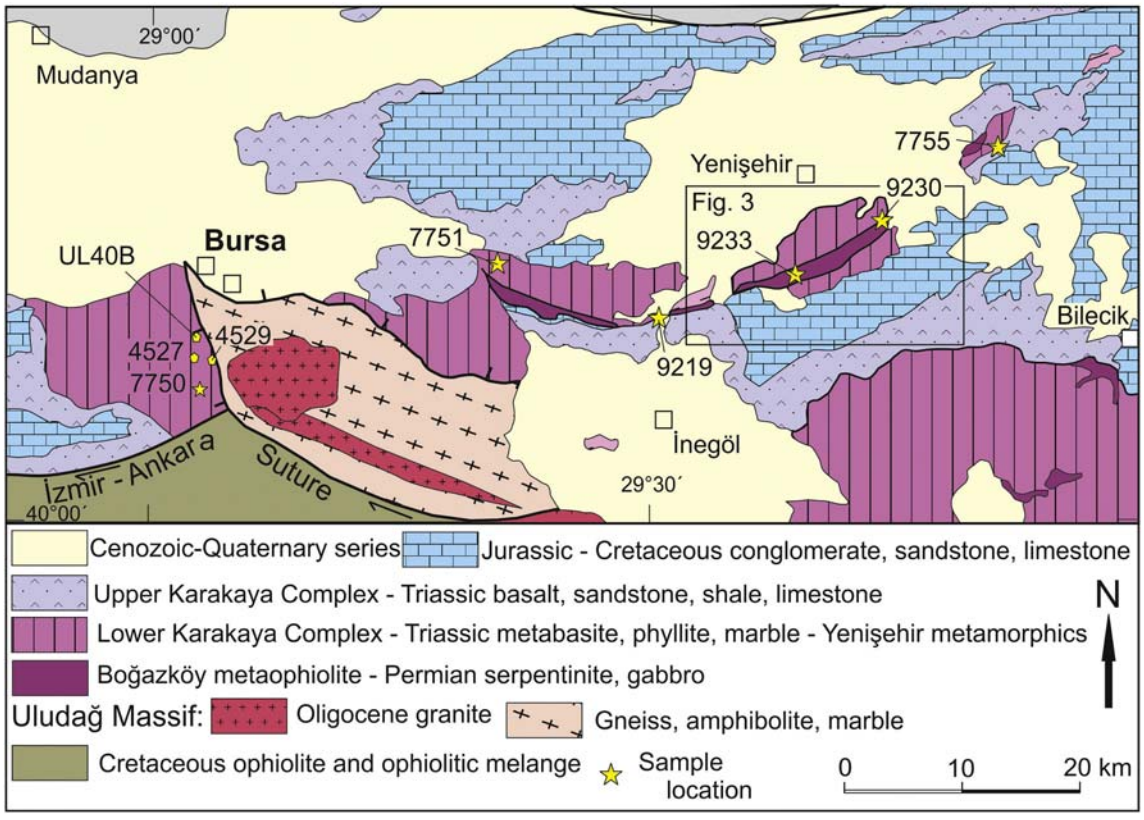

Fig. 2. Geological map of the Yenişehir area together with the sample locations. (Modified after Türkecan and Yurtsever, 2002.)

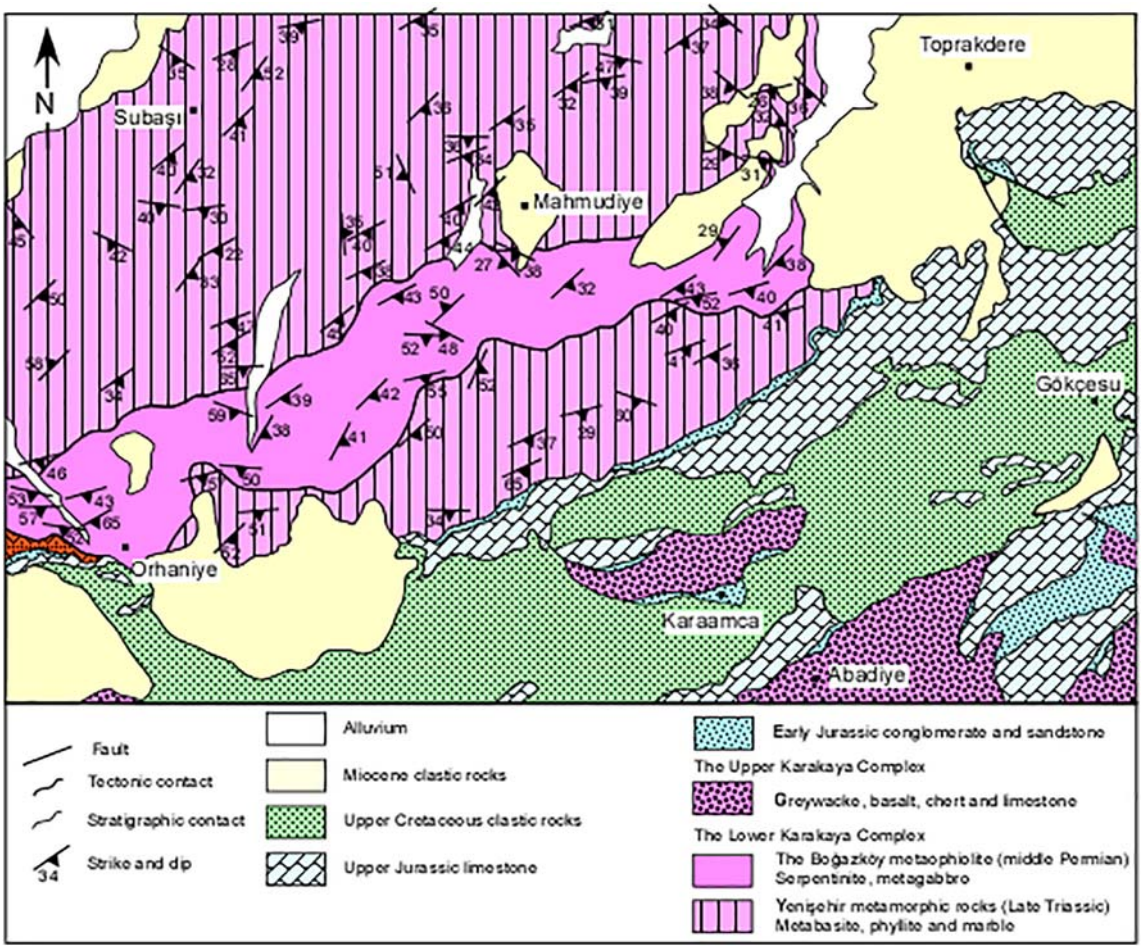

Fig. 3. Detailed map of the Bogazköy metaophiolite and the Yenişehir metamorphic rocks (modified after Genç, 1993). For location see Fig. 2.

rocks and the Boğazköy meta-ophiolite are concordant, mainly trending in NE-SW, and dipping to SE at 40–60°. The meta-ophiolite is made up of serpentinite (nearly 90% of the outcrop area), and metagabbro. The serpentinite is grey to dark green, and moderately to strongly foliated/sheared (Fig. 4a–b), and locally converted into massive carbonate-quartz rock. The metagabbros form small stocks up to 10 m in diameter, or boudinaged dykes with strongly sheared margins (Fig. 4c–d). The metagabbros are pale green and show a well-developed foliation and medium-grain size. There are locally pegmatitic metagabbro domains with thicknesses up to 20 cm (Fig. 4e–f). In some places, the foliation is feeble to absent. The foliations in both the metagabbro and the serpentinite are concordant, indicating a common history of deformation and metamorphism.

3. Analytical techniques

Mineral analyses were carried out with a CAMECA SX51 electron microprobe equipped with five wavelength-dispersive spectrometers at the Institute of Earth Sciences at Heidelberg. Standard operating conditions were 15 kV accelerating voltage, 20 nA beam current and a beam diameter of ~1 μm. Feldspars were analysed with a defocused beam (10 μm) to minimise loss of alkalis. Counting times were usually 10 s except for Mg, Ca and Al (20 s) and Ti (30 s) in magnetite and ilmenite. Natural and synthetic oxide and silicate standards were used for calibration. The PAP algorithm was applied to raw data. On the other hand, the Cr-Al spinel analyses were carried out with a CAMECA SX100 electron microprobe equipped with four wavelength-dispersive spectrometers and one Brooker energy dispersive system at the Adnan Tekin research center (Istanbul Technical University). Operation conditions were 10 kV, and 10 nA, and 5 μm beam size. Counting times were 20 s on peak and on background. Calibration has been performed on synthetic and natural oxide and silicate standards.

For bulk-rock analyses about 3 kg of metagabbro were first processed in a steel jaw crusher and an aliquot of about 30 g was powdered in an agate rind-disc mill. Rock powders were then dried at 105 °C for about 24 h. 200 mg of rock powder were mixed with 1.5 g of $LiBO_2$ flux in a graphite crucible. Subsequently, the crucible was placed in an oven and heated to 1050 °C for 15 min. The molten samples were dissolved in 5% HNO_3 (ACS grade nitric acid diluted in demineralised water). International reference samples (NCSDC71301, AGV-2 and W2A) and reagent blanks were added to the sample sequence, and analysed together with the samples. For analyses of major elements, sample solutions were aspirated into an ICP emission spectrograph (Jarrel Ash AtomComb 975) at Acme Analytical Laboratories Ltd. in Vancouver, Canada. For the determination of trace elements including rare earth elements, the solutions were aspirated into an ICP mass spectrometer (Perkin-Elmer Elan DRC-e) at the Geochemical Laboratory of the Kocaeli University, Turkey. Analysis of the international reference materials (NCSDC71301, AGV-2 and W2A) together with the certified values and blank values for each element are given in Appendices Table A1.

Zircon separation and preparation of epoxy mounts were performed in the Eurasia Institute of Earth Sciences in Istanbul Technical University. The separation was carried out by conventional techniques including crashing, sieving, magnetic and heavy liquid separation, picking under binocular. Zircons were selected under binocular, and embedded in epoxy. Mounted zircons were polished up to half-thickness until grains were exposed. Mounted zircons were imaged by means of cathode-luminescence in the geology department of the Hacettepe University

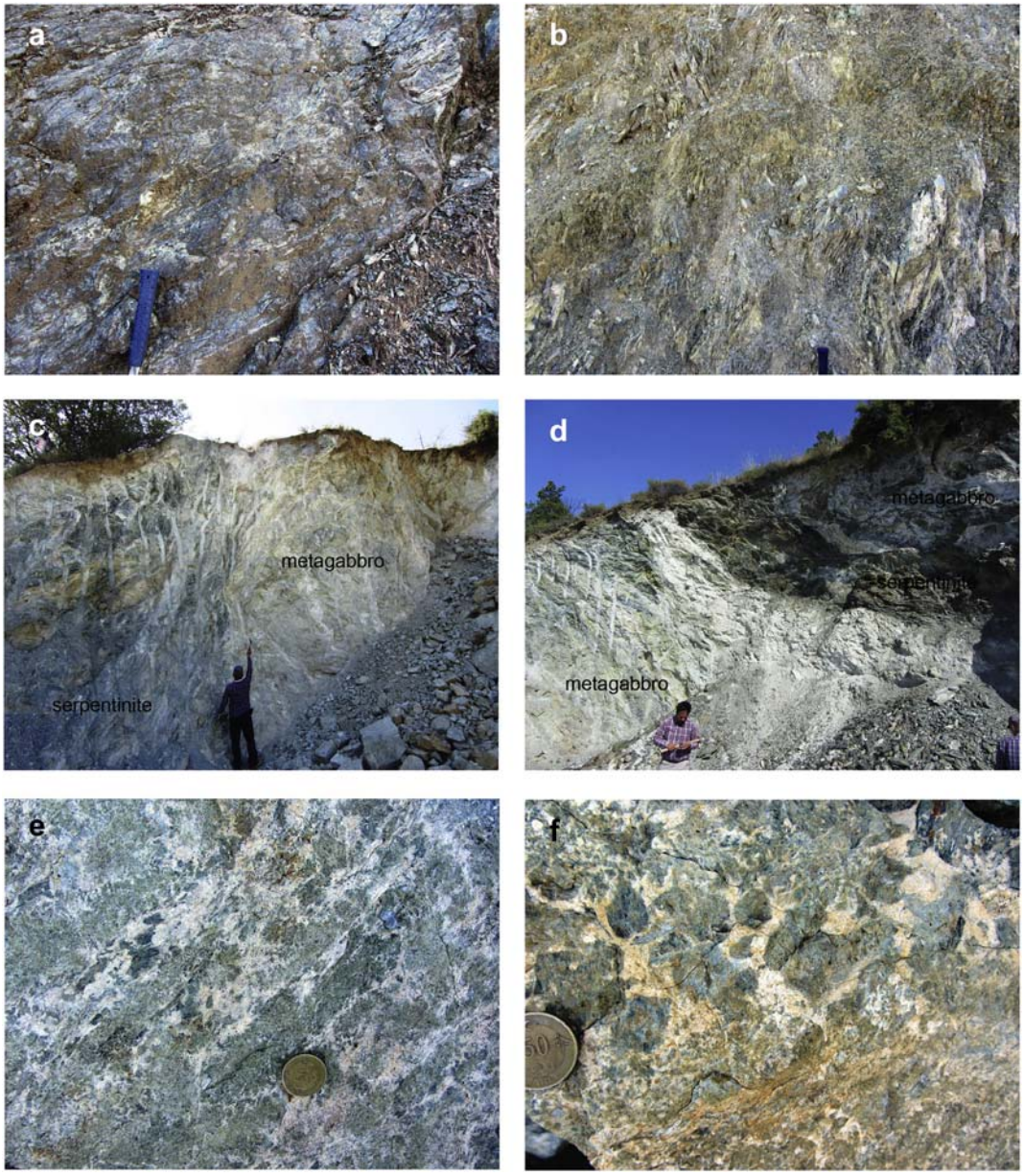

Fig. 4. Field photographs of (a–b) strongly foliated serpentinite, (c–d) gabbroic stocks in serpentinite, (e) close-up picture of metagabbro, and (f) pegmatitic domain in a metagabbro.

(Ankara) by ZeissEvo-50SEM equipped with cathode-luminescence and EDS detectors, to characterise the zircons before the in-situ LA-ICP-MS dating. U-Pb zircon dating was performed by laser ablation split-stream inductively coupled plasma mass spectrometry (LASS-ICP-MS), using a Nu Plasma multicollector ICP-MS for U/Th-Pb data and an Agilent 7700 quadrupole ICP-MS for trace-element concentration, following the methods of Kylander-Clark et al. (2013). Samples were ablated using a Photon Machines Excite excimer laser system with a spot size of 25 μm, a repetition rate of 4 Hz and an approximate fluence of 1 J/cm^2. Data were processed with *Iolite* version 2.5 (Paton et al., 2011), and plotted with *Isoplot* (Ludwig, 2003).

Muscovite-phengite separation for $^{40}Ar/^{39}Ar$ dating was performed by conventional techniques including crashing, sieving and magnetic separation at the Eurasian Institute of Earth Sciences in Istanbul. The samples were then irradiated at the BER II reactor at the Helmholtz Zentrum in Berlin. $^{40}Ar/^{39}Ar$ dating was carried out at the Institut für Geowissenschaften, Universität Heidelberg with a MAT GD-150 gas mass spectrometer (0.38 T permanent magnet, 180°, 5 cm radius of curvature), with no detectable background. Gas amounts were corrected for mass discrimination, furnace and line blanks, as well as for irradiation interferences ($(^{36}Ar/^{37}Ar)_{Ca} = (4.32 \pm 0.19) \cdot 10^{-4}$; $(^{39}Ar/^{37}Ar)_{Ca} = (9.80 \pm 0.31) \cdot 10^{-4}$; $(^{40}Ar/^{39}Ar)_{K} = (1.5 \pm 0.4) \cdot 10^{-2}$; $(^{38}Ar/^{39}Ar)_{K} = (1.79 \pm 0.01) \cdot 10^{-2}$). Ages were calculated using the fluence monitor Bmus/2 muscovite ($t = 328.5 \pm 1.1$ Ma (1σ), Schwarz and Trieloff, 2007) and the recommended decay constants by Steiger and Jäger (1977). Errors in parentheses include the uncertainty of the fluence monitor. When using the most recently suggested values for the K decay constants (Renne et al., 2010, 2011; Schwarz et al., 2011, 2012) the Ar-Ar ages would increase by about 1%. All uncertainties in this study are on a 2σ uncertainty level, unless stated differently. Coordinates of the samples mentioned in the text are given in Appendices Table A2.

4. Petrography and mineral compositions

Over 50 samples from the Boğazköy metaophiolite and the Yenişehir metamorphic rocks were examined petrographically. Six representative samples were analysed by electron microprobe for mineral compositions.

4.1. Serpentinite

Serpentinite is generally well foliated, and consists of serpentine, ferrichromite-magnetite, ±chlorite, ±talc and ±calcite and relict Cr-Al spinel. Primary peridotite texture is mostly obliterated (Fig. 5a). X-ray powder diffraction studies on five serpentinite samples (9227, 9230B, 9235C, 9236 and 9237A) indicated that the main serpentine mineral is antigorite. Only samples 9235C and 9236 contain additional trace amounts of lizardite. The only relict mineral is Cr-Al spinel which was replaced by ferrichromite to magnetite along the margins and fractures (Fig. 5b). Compositionally, the Cr-Al spinels are characterised by (i) Cr/(Cr + Al) values of 0.45–0.55, and wide-ranging Mg/(Mg + Fe^{2+}) values of 0.76 to 0.22, (ii) extremely low TiO_2 contents, and (iii) variable contents of ZnO and MnO (Fig. 6a–d; Table 1). Mn and Zn are positively correlated, and display a negative correlation with Mg. These chemical features can be accounted for by Mn and Zn substitution for Mg, leading to large variation in Mg/(Mg + Fe^{2+}) values, which probably occurred during the greenschist- to blueschist-facies metamorphism. Therefore, the most magnesian compositions approximate to the primary composition (e.g. Mg/(Mg + Fe^{2+}) = 0.45–0.55). Similar Cr- and Mn-rich Cr-Al spinels were described from the serpentinites of the Tidding suture (eastern Himalaya, India) by Singh and Singh (2013). The Cr/(Cr + Al) and Mg/(Mg + Fe^{2+}) of the Cr-Al spinels are similar to those found in both abyssal and fore-arc peridotites (Fig. 5a). However, the spinels differ from those in the abyssal peridotites with their low TiO_2 contents (0.01–0.06 wt%) (Fig. 6d).

4.2. Metagabbro

The metagabbro is fine- to medium-grained (0.3 to 2 mm), and displays a feeble to strong foliation. Main minerals in the metagabbro are actinolite/winchite, epidote, chlorite, albite, titanite and phengite (Fig. 5c; Table 2). Accessory phases are apatite and zircon. This mineral assemblage is comparable to that in the metabasic rocks of the Yenişehir metamorphic rocks. Actinolite/winchite is characterised by Si contents of 7.31–7.61 cations per 23 oxygens, Na/Ca ratios of 0.31–0.59, respectively. Epidotes display Fe^{3+}/(Fe^{3+} + Al) ratios of 0.19–0.21. Chlorite displays X_{Mg} values of 0.77–0.78, and contains trace amounts of Mn.

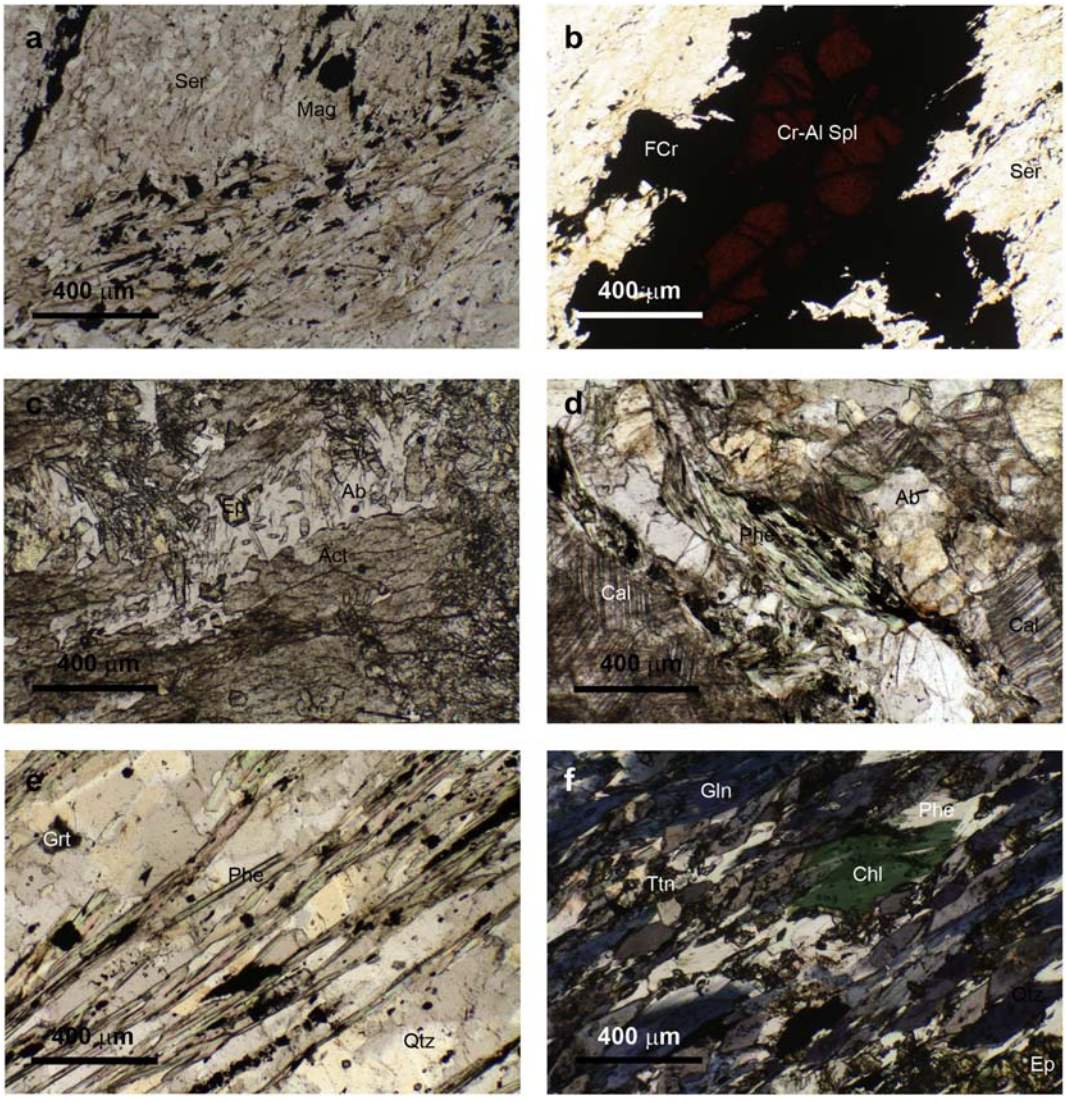

Fig. 5. Thin section micrographs showing microtextural features of the Boğazköy metaophiolite and the Yenişehir metamorphic rocks. a Flakes of serpentine (Ser) intergrown with ferrichromite to magnetite (FCr) (sample 9235C), b relict Cr-Al spinel (Spl) overgrown by ferrichromite to magnetite (FCr) in serpentinite (sample 9230B), c irregular intergrowth of actinolite/winchite (Act), epidote (Ep) and albite (Ab) in metagabbro (sample 9218A), d Phengite (Phe), Quartz (Qtz) and albite in calc-schist (sample 7750). Phengite is intergrown with hematite and kaolinite, e Phengite and tiny grain of garnet (Grt) in metachert (sample 7751), f Well-developed foliation in calcite-bearing blueschist (sample 7755B). Gln: Glaucophane, Chl: Chlorite.

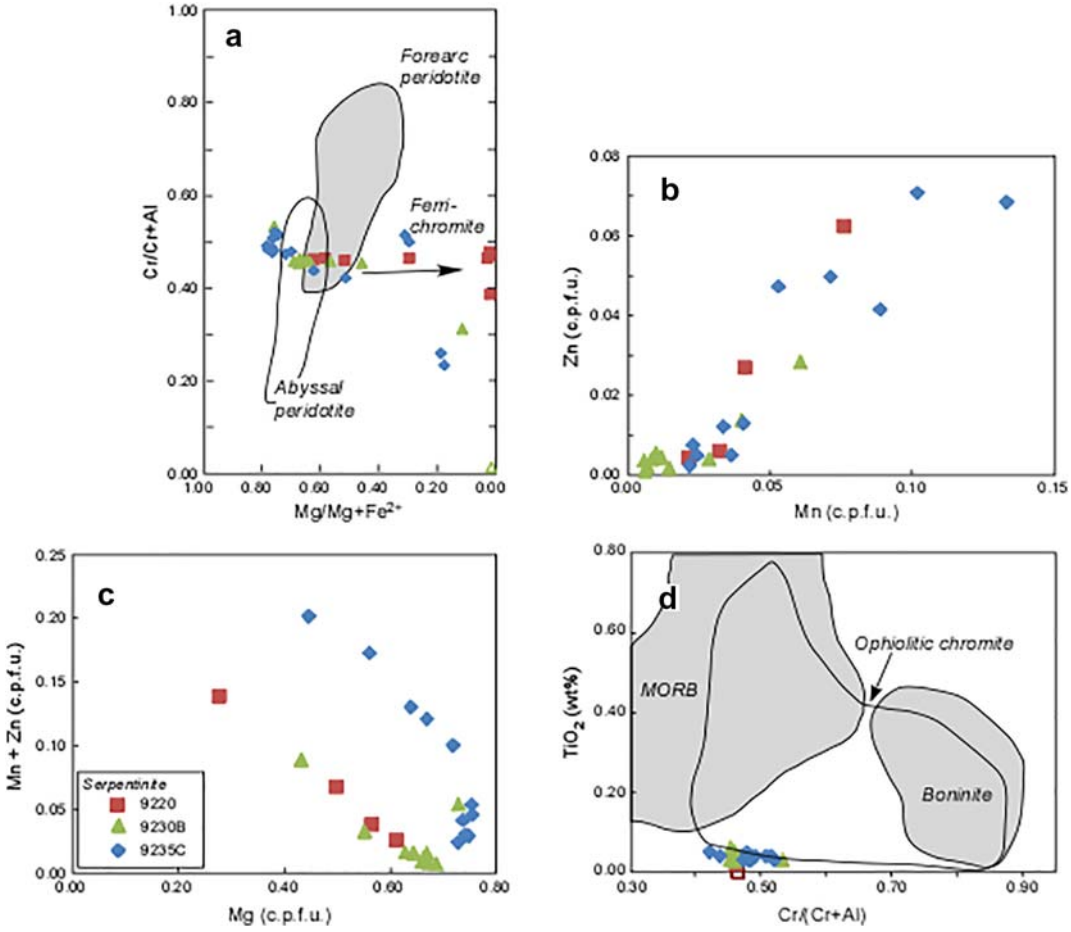

Fig. 6. Compositional variation of Cr-Al spinels, ferrichromites and magnetite in the Boğazköy serpentinite: a $Mg/(Fe^{2+}+Mg)$ vs. $Mg/(Mg + Fe^{2+})$. Fields of abyssal and forearc peridotite are after Dick and Bullen (1984), b positive correlation between Mn and Zn contents of the Cr-Al spinels, c negative variation between Mg and Mn + Zn contents of the Cr-Al spinels, and d $Cr/(Cr + Al)$ vs. TiO_2 diagram. The enclosed fields are from Huang et al. (2017) and the references therein.

Phengite is characterised by Si contents of 3.27–3.28 cations per 11 oxygens. Titanite displays Al_2O_3 and Fe_2O_3 ^{tot} contents of 1.00–1.32 and 0.40–0.53 wt%, respectively. Albite has nearly end-member compositions ($An_{\leq 04}$).

5. Bulk rock compositions

Four samples from the serpentinite and nine samples from the metagabbro were analysed for major and trace element compositions

Table 1
Selected electron microprobe analyses of Cr-Al spinel (Spl), ferrichromite (FCr) and magnetite (Mag) from the Boğazköy serpentinite (NW Turkey).

Sample	9220	9220	9220	9220	9230B	9230B	9230B	9230B	9230B	9235C	9235C	9235C	9235C	9235C
Mineral	Spl	Spl	FCr	FCr	Spl	Spl	Spl	CrMag	Mag	Spl	Spl	Spl	FCr	Mag
TiO_2	0.00	0.02	0.09	0.09	0.04	0.03	0.06	0.34	0.11	0.04	0.03	0.03	0.07	0.07
Al_2O_3	27.8	29.74	1.67	3.02	28.23	29.02	25.64	0.54	0.04	26.27	23.85	28.09	0.22	0.01
Cr_2O_3	37.17	39.29	31.33	32.06	38.44	39	36.53	20.01	0.86	44.11	39.83	41.49	34.11	17.25
FeO	23.29	15.85	54.4	51.66	17.17	14.96	23.51	65.32	88.62	12.14	16.53	11.75	48.01	67.27
MnO	2.86	0.87	4.01	4.15	0.59	0.26	2.3	2.67	0.23	0.89	2.82	0.94	7.51	4.97
MgO	5.83	13.76	0.36	0.35	13.97	15.49	9.2	1.83	0.26	16.51	14.91	16.93	4.13	2.81
ZnO	2.68	0.21	3.82	4.48	0.09	0.06	1.23	0.59	0.21	0.12	2.25	0.36	1.5	0.92
Total	99.63	99.74	95.68	95.81	98.53	98.82	98.47	91.3	90.33	100.08	100.22	99.59	95.55	93.28
Ti	0.000	0.000	0.003	0.003	0.001	0.001	0.001	0.010	0.003	0.001	0.001	0.001	0.002	0.002
Al	1.038	1.043	0.075	0.134	1.004	1.017	0.950	0.025	0.002	0.915	0.846	0.973	0.010	0.000
Cr	0.931	0.925	0.940	0.956	0.917	0.917	0.908	0.618	0.027	1.031	0.947	0.964	0.998	0.518
Fe^{3+}	0.032	0.031	0.980	0.904	0.078	0.065	0.138	1.337	1.965	0.052	0.206	0.061	0.988	1.479
Fe^{2+}	0.585	0.363	0.746	0.725	0.356	0.306	0.480	0.798	0.974	0.248	0.210	0.228	0.498	0.657
Mn	0.077	0.022	0.129	0.133	0.015	0.007	0.061	0.088	0.008	0.022	0.072	0.023	0.235	0.160
Ni	0.000	0.000	0.000	0.000	0.000	0.000	0.000	0.000	0.000	0.000	0.000	0.000	0.000	0.000
Mg	0.275	0.611	0.020	0.020	0.628	0.686	0.431	0.107	0.015	0.728	0.669	0.742	0.228	0.159
Zn	0.063	0.005	0.107	0.125	0.002	0.001	0.029	0.017	0.006	0.003	0.050	0.008	0.041	0.026
Total	3.000	3.000	3.000	3.000	3.000	3.000	3.000	3.000	3.000	3.000	3.000	3.000	3.000	3.000
$Mg/(Mg + Fe^{2+})$	0.30	0.62	0.02	0.02	0.64	0.69	0.46	0.12	0.02	0.74	0.72	0.76	0.30	0.19
$Cr/(Cr + Al)$	0.47	0.46	0.47	0.48	0.46	0.46	0.45	0.31	0.01	0.52	0.47	0.48	0.50	0.26

Table 2
Selected analyses of minerals in metagabbro from the Boğazköy metaophiolite, NW Turkey.

Sample	9227B	9227B	9227B	9227B	9227B	9227B	9227B	9227B	9227B	9227B
Mineral	Amp	Amp	Amp	Amp	Ep	Ep	Phe	Phe	Chl	Chl
SiO_2	52.90	54.43	52.65	53.67	37.81	38.40	48.73	48.92	28.57	28.48
TiO_2	0.09	0.03	0.11	0.04	0.08	0.11	0.23	0.15	0.02	0.00
Al_2O_3	5.92	3.93	6.44	4.03	26.20	26.55	28.07	28.71	21.06	20.85
Cr_2O_3	0.01	0.05	0.00	0.04	0.10	0.04	0.13	0.03	0.05	0.01
FeO	9.35	8.06	8.87	8.13	9.53	8.97	2.76	2.60	12.55	12.74
MnO	0.21	0.22	0.27	0.20	0.24	0.21	0.01	0.03	0.23	0.22
MgO	16.75	18.42	16.53	18.08	0.03	0.02	4.07	3.87	25.01	24.98
CaO	9.47	11.10	9.31	10.87	23.58	23.81	0.01	0.02	0.01	0.00
Na_2O	3.07	1.93	3.01	1.98	0.02	0.02	0.44	0.46	0.00	0.02
K_2O	0.30	0.16	0.19	0.17	0.01	0.01	10.74	10.75	0.02	0.01
Total	98.07	98.32	97.39	97.20	97.58	98.15	95.19	95.54	87.52	87.31
Cations on the basis of 13 oxygens excluding Ca, Na and K					12.5 O	12.5 O	11 O	11 O	14 O	14 O
Si	7.401	7.567	7.391	7.551	2.960	2.982	3.284	3.279	2.808	2.809
Ti	0.009	0.003	0.012	0.004	0.005	0.007	0.012	0.008	0.002	0.000
Al	0.976	0.644	1.065	0.668	2.418	2.430	2.229	2.267	2.439	2.424
Cr	0.001	0.005	0.000	0.004	0.006	0.003	0.007	0.001	0.004	0.001
Fe^{+3}	0.477	0.355	0.477	0.370	0.624	0.583	0.000	0.000	0.000	0.000
Fe^{+2}	0.617	0.581	0.564	0.586	0.000	0.000	0.155	0.146	1.031	1.051
Mn	0.025	0.026	0.032	0.024	0.016	0.014	0.001	0.002	0.019	0.018
Mg	3.494	3.818	3.459	3.792	0.004	0.003	0.409	0.387	3.664	3.673
Ca	1.419	1.653	1.400	1.638	1.978	1.981	0.001	0.001	0.001	0.000
Na	0.833	0.520	0.819	0.540	0.003	0.003	0.058	0.060	0.000	0.003
K	0.054	0.028	0.034	0.031	0.000	0.001	0.923	0.919	0.003	0.001
X_{Mg}	0.85	0.87	0.86	0.87	–	–	0.72	0.73	0.78	0.78
X_{Fe3}	–	–	–	–	0.21	0.19	–	–	–	–

(Table 3). Seeing that the Boğazköy meta-ophiolite fragment underwent a greenschist- to blueschist-facies metamorphism, the effect of metamorphism on the element mobility of major and trace elements is important. Several studies indicated that elements such as Na, K, Ca, Rb, Sr and Ba are highly mobile during metamorphic events (e.g., Polat and Hofmann, 2003). Rare earth elements (REE), high-field strength elements (Th, Nb, Ta, Zr, Hf and Ti) and transitional metal elements (Sc, V, Cr and Ni) are commonly regarded as immobile during metamorphism (e.g. Ghatak et al., 2012; Pearce, 2014; Polat and Hofmann, 2003). On the other hand, in the focused flow settings such as veins and lithological contacts, both rare earth elements and high-field strength elements are mobilised (Ague, 2017). Special care was given during the sampling. The samples were taken away from any late veins and lithological contacts.

5.1. Serpentinite

The loss on ignition values of the serpentinite samples range from 11 to 13 wt%, in line with their totally hydrated nature. The samples display similar refractory compositions (Table 3). Ni, Cr, Co and V contents are extremely high. Consistently low Al_2O_3 and CaO contents indicate that the primary peridotite was probably clinopyroxene-poor, i.e. a depleted harzburgite or dunite. Their Mg# values ($=100 * \text{molar MgO}/(\text{MgO} + \text{FeO}_{tot})$) are 90–91. The serpentinites display chondrite-normalised REE patterns with enrichments of light and heavy REEs relative to middle REE, resulting in concave U-shaped patterns with positive Eu anomalies ($Eu/Eu^* = Eu_{cn}/(Sm_{cn} * Gd_{cn})^{0.5} = 1.28–2.62$) (Fig. 7a). Only sample 9230B is devoid of a Eu anomaly.

5.2. Metagabbro

Loss on ignition values range from 1.90 to 3.40 wt% (Table 3). On a volatile-free basis, the metagabbros are characterised by SiO_2 and Al_2O_3 contents of 47–54 and 15–18 wt%, respectively. Mg# values are extremely high, ranging from 75 to 88. MgO, CaO and Na_2O contents are variable (Fig. 8). Ni and Cr contents increase with increasing Mg#. TiO_2, P_2O_5 and Zr contents are low. Chondrite-normalised REE patterns show strong variations of $(La/Yb)_{cn}$ (0.48–3.05) and positive Eu/Eu* values of 1.33–1.60 (Fig. 7b). Eu/Eu* values are not correlated with the Sr content, implying that Sr budget is not controlled wholly by plagioclase. Compositional features, such as (i) variable CaO and MgO contents, (ii) anomalously high Mg# and low contents of incompatible elements such as Ti, P and Zr, and (iii) positive Eu anomalies point to derivation from plagioclase-clinopyroxene cumulates from which a derivative liquid has been expelled.

6. Zircon geochemistry

Despite low Zr contents in the bulk compositions (6 to 62 μg/g; Table 3), at least twenty grains of zircon were found in 10 kg metagabbro samples (sample numbers: 9219, 9230 and 9233). Their trace element compositions (REE, Ti, Nb, Hf, Th, U, Y, and P) were measured concurrently with U-Pb age data at the same spot (cf. Appendices Tables A3 and A4). The following discussion is based on 105 point analyses.

The analysed zircon grains are characterised by prismatic euhedral forms with sizes of 60–140 μm along the c axis, and display oscillatory and sector zoning (Fig. 9a). Measured trace-element concentrations display wide variations (Appendices Table A3). The least variation in the measured trace-element abundances occur in sample 9219, and the greatest one in sample 9233. Some of this variation might have been caused by (i) the presence of micro-inclusions, (ii) fluid-modified, altered domains or (iii) hydrothermal zircon growth (e.g. Hoskin, 2005). The following description is based on the analysis which were screened for possible microinclusions and hydrothermally altered domains. The screening procedure is given in the Appendix A1.

The Th/U ratios are in the range 0.38–1.55, comparable to zircons grown from a melt phase (Hoskin and Schaltegger, 2003). Concentrations of Yb (348–1790 μg/g) are high relative to those of U (35–424 μg/g), resulting in relatively low U/Yb ratios which is characteristic of zircons from the oceanic crust (c.f. Grimes et al., 2007). REE patterns of zircons, normalised to chondrite values (Boynton, 1984) are characterised by (i) enrichments of the heavy rare earth elements with respect to the light rare earth elements ($(Lu/Pr)_{cn} = 302–7149$; $(Lu/Gd)_{cn} = 14–43$), (ii) negative Eu anomaly ($Eu/Eu^* = 0.25–0.53$), and (iii) pronounced positive Ce anomaly ($Ce/Ce^* = Ce_{cn}/(La_{cn} * Pr_{cn})^{0.5} = 7–172$) (Fig. 9b–d). A positive Ce anomaly is commonly ascribed to oxidation of Ce^{3+} to Ce^{4+} which fits better into the structure

Table 3
Whole-rock analyses of selected samples from the metagabbros in the Boğazköy metaophiolite fragment, NW Turkey.

Sample	9218A	9218B	9219	9219B	9230A	9233	9234A	9235A	9235B	9230B	9235C	9236	9237A
Rock type	MG	MG	MG	MG	MG	MG	MG	MG	MG	SER	SER	SER	SER
Oxides in wt%													
SiO_2	48.59	47.69	47.25	44.60	49.72	51.63	50.50	49.94	49.64	38.54	36.34	36.51	36.56
TiO_2	0.18	0.23	0.25	0.11	0.36	0.31	0.19	0.29	0.28	0.05	0.05	0.01	0.03
Al_2O_3	14.96	16.70	17.21	16.94	16.42	16.50	14.33	16.17	17.09	1.06	0.79	1.01	1.11
$Fe_2O_3^{tot}$	4.42	4.41	4.38	3.47	6.34	5.37	5.27	5.42	4.89	7.84	7.55	7.84	7.68
MnO	0.11	0.09	0.08	0.29	0.12	0.14	0.13	0.15	0.11	0.18	0.20	0.19	0.20
MgO	12.87	11.45	11.22	12.50	9.58	9.84	11.50	10.01	9.02	40.88	44.12	41.70	42.73
CaO	13.48	14.52	14.23	16.99	12.63	8.55	11.67	12.14	14.87	0.11	0.06	0.07	0.03
Na_2O	1.43	1.39	1.50	0.52	1.81	3.05	3.02	2.61	1.85	0.06	0.05	0.03	0.05
K_2O	0.07	0.13	0.08	0.19	b.d.	0.98	0.12	0.19	0.05	b.d.	b.d.	b.d.	b.d.
P_2O_5	0.01	b.d.	0.02	b.d.	0.03	0.02	b.d.	b.d.	0.01	0.01	0.01	b.d.	b.d.
LOI	3.40	2.90	3.30	3.90	2.70	3.40	2.90	2.80	1.90	11.31	11.73	12.55	11.58
Total	99.52	99.51	99.52	99.51	99.71	99.79	99.63	99.72	99.71	100.03	100.89	99.92	99.97
Trace elements in μg/g													
Sc	32	33	28	30	33	36	42	37	36	n.m.	n.m.	n.m.	n.m.
Ni	291	226	298	358	161	98	192	119	123	1331	1636	1946	1819
Cr	1637	1582	1585	1518	490	162	517	209	401	2481	2430	2906	2459
Co	35	30	36	33	36	31	33	36	27	173	59	90	100
V	121	136	125	126	173	181	192	197	174	96	29	30	50
Cu	41.1	43.5	33.4	54.1	27.8	32.3	33.5	60.5	66.2	12.9	3.5	5.8	43.5
Zn	5	8	6	17	12	18	7	29	6	49	67	51	50
Cs	0.047	0.096	0.232	0.310	0.008	0.401	0.076	0.032	0.011	0.010	<0.005	<0.005	<0.005
Rb	0.5	1.0	0.7	1.4	0.3	9.3	1.0	2.0	0.7	0.2	0.1	0.02	0.1
Ba	3.4	9.4	9.0	41.8	8.6	69.9	12.1	22.9	9.2	4.5	1.8	1.3	1.0
U	<0.005	<0.005	0.032	<0.005	0.018	0.046	0.015	0.006	0.008	0.011	0.047	0.261	0.061
Th	<0.01	<0.01	0.26	<0.01	0.08	0.17	0.06	0.03	0.03	0.13	0.05	<0.01	<0.01
Pb	0.07	0.24	0.11	1.17	1.09	0.21	0.89	0.08	0.05	1.08	0.08	<0.03	0.20
Sr	70.5	84.8	83.8	208.3	81.0	88.2	118.9	79.4	103.3	0.8	0.6	0.6	0.5
Nb	0.106	0.147	2.061	0.072	0.876	2.052	0.511	0.285	0.361	0.077	0.027	0.026	0.022
Ta	0.010	0.021	0.180	0.005	0.060	0.139	0.037	0.023	0.027	0.005	<0.002	<0.002	<0.002
Zr	6.4	13.2	62.0	4.4	16.0	20.9	7.3	9.5	11.4	4.3	2.5	2.0	1.7
Hf	0.2	0.4	1.4	0.2	0.5	0.5	0.3	0.3	0.4	0.1	0.1	0.1	0.1
Y	5.0	6.5	9.0	4.1	8.8	8.2	6.5	8.5	7.5	0.6	0.3	0.3	0.4
La	0.153	0.248	1.031	0.268	1.102	1.224	0.495	0.421	0.715	0.291	0.105	0.072	0.058
Ce	0.579	0.939	2.670	0.633	2.588	2.598	1.173	1.306	1.473	0.474	0.275	0.101	0.136
Pr	0.123	0.197	0.425	0.106	0.430	0.448	0.219	0.252	0.289	0.080	0.034	0.020	0.027
Nd	0.801	1.206	2.230	0.655	2.189	2.247	1.223	1.556	1.645	0.330	0.141	0.130	0.160
Sm	0.366	0.517	0.786	0.275	0.773	0.789	0.516	0.676	0.657	0.081	0.034	0.020	0.027
Eu	0.256	0.285	0.437	0.235	0.432	0.516	0.314	0.447	0.416	0.021	0.016	0.014	0.019
Gd	0.434	0.577	0.844	0.333	0.755	0.726	0.528	0.666	0.624	0.060	0.021	0.017	0.018
Tb	0.098	0.128	0.179	0.074	0.162	0.159	0.126	0.150	0.143	0.011	0.004	0.004	0.004
Dy	0.797	0.989	1.439	0.647	1.390	1.288	1.070	1.289	1.187	0.090	0.037	0.033	0.040
Ho	0.179	0.229	0.317	0.141	0.304	0.282	0.249	0.295	0.263	0.016	0.007	0.009	0.009
Er	0.504	0.677	0.960	0.408	0.947	0.830	0.712	0.841	0.762	0.049	0.020	0.025	0.025
Tm	0.073	0.095	0.139	0.059	0.135	0.115	0.102	0.122	0.112	0.007	0.003	0.005	0.005
Yb	0.495	0.648	0.905	0.355	0.917	0.774	0.701	0.819	0.748	0.058	0.029	0.027	0.040
Lu	0.067	0.096	0.144	0.049	0.118	0.106	0.091	0.114	0.106	0.010	0.006	0.008	0.007
Mg#	85.21	83.72	83.53	87.69	74.94	78.39	81.19	78.52	78.49	90.29	91.24	90.46	90.84
(La/Yb)cn	0.21	0.26	0.76	0.52	0.81	1.07	0.48	0.35	0.65	3.36	2.47	1.80	0.97
Eu/Eu*	1.99	1.61	1.65	2.31	1.73	2.09	1.81	2.04	2.01	0.93	1.78	2.29	2.62

Oxides are given in weight % and trace elements in μg/g. MG metagabbro; SER serpentinite; cn chondrite-normalised; b.d. below detection; $Eu/Eu^* = Eu_{cn}/(Sm_{cn} \cdot Gd_{cn})^{0.5}$; Mg# = 100 * molar MgO/(MgO + FeO*).

of zircon (Hinton and Upton, 1991; Kaczmarek et al., 2008), and negative Eu anomaly to the formation from an Eu depleted melt due to the crystallisation of plagioclase. The Eu anomaly does not show any linear relationship with Ce anomaly and Ti contents (not shown), thus ruling out zircon formation from gradually oxidizing evolved melt.

To summarise, both topological and compositional features of the analysed zircon grains point to growth from a melt phase after the crystallisation of some plagioclase.

7. Geochronology

To constrain the formation age of the ophiolite and the timing of greenschist- to blueschist-facies metamorphism, U-Pb dating has been carried out on zircons from three metagabbro samples (9219, 9230 and 9233). In addition, stepwise ^{40}Ar-^{39}Ar dating on phengite from three samples of the Yenişehir metamorphic rocks (7750, 7751 and 7755B) was performed. Sample locations are shown in Fig. 2. Analytical data are given in Appendices Tables A4 and A5.

7.1. LA-ICP-MS zircon dating

In the U-Pb age calculations, only the analyses with concordance values ($^{206}Pb/^{238}U$ age divided by $^{207}Pb/^{235}U$ age) between 0.95 and 1.05 are used, and analyses of hydrothermally altered domains were excluded from the calculations. The analyses form relatively tight clusters on the Terra-Wasserburg plot (Fig. 10; Appendices Table A4). 22 analyses from sample 9219 gave an intercept age value of 262 ± 5 Ma (2σ; MSWD = 0.98). 13 analyses from sample 9230 yielded a similar value of 264 ± 3 Ma (2σ; MSWD = 0.26). Furthermore, 28 analyses from sample 9233 recorded a value of 258 ± 5 Ma (2σ; MSWD = 1.2). These ages correspond to the Capitanian (late Guadalupian, middle Permian) (Cohen et al., 2013). On the basis of (i) topological and

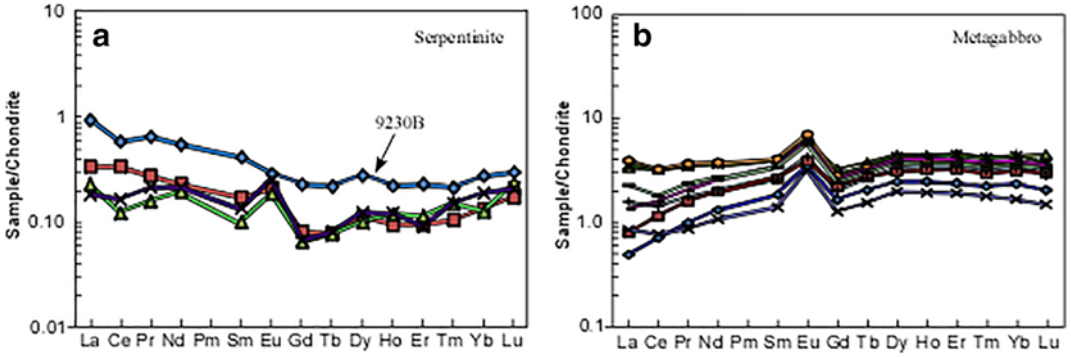

Fig. 7. Chondrite normalised REE patterns of (a) the serpentinites, and (b) metagabbros from the Boğazköy metaophiolite. The normalisation values are from Boynton (1984).

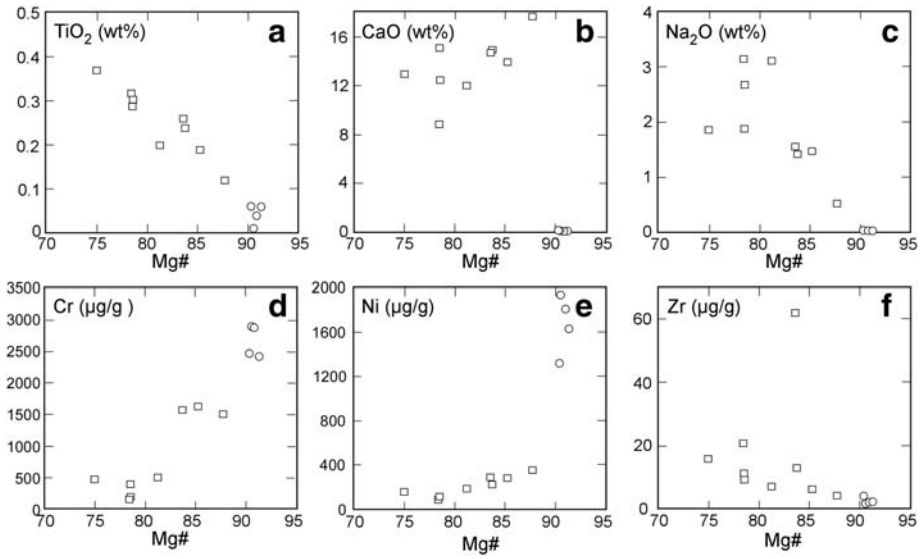

Fig. 8. Major and trace element diagrams of the metagabbros within the Boğazköy metaophiolite. a Mg# (=100 * molar MgO/(MgO + FeO_{tot})) vs. TiO_2, b Mg# vs. CaO, c Mg# vs. Na_2O, d Mg# vs. Cr, e Mg# vs. Ni, and f Mg# vs. Zr.

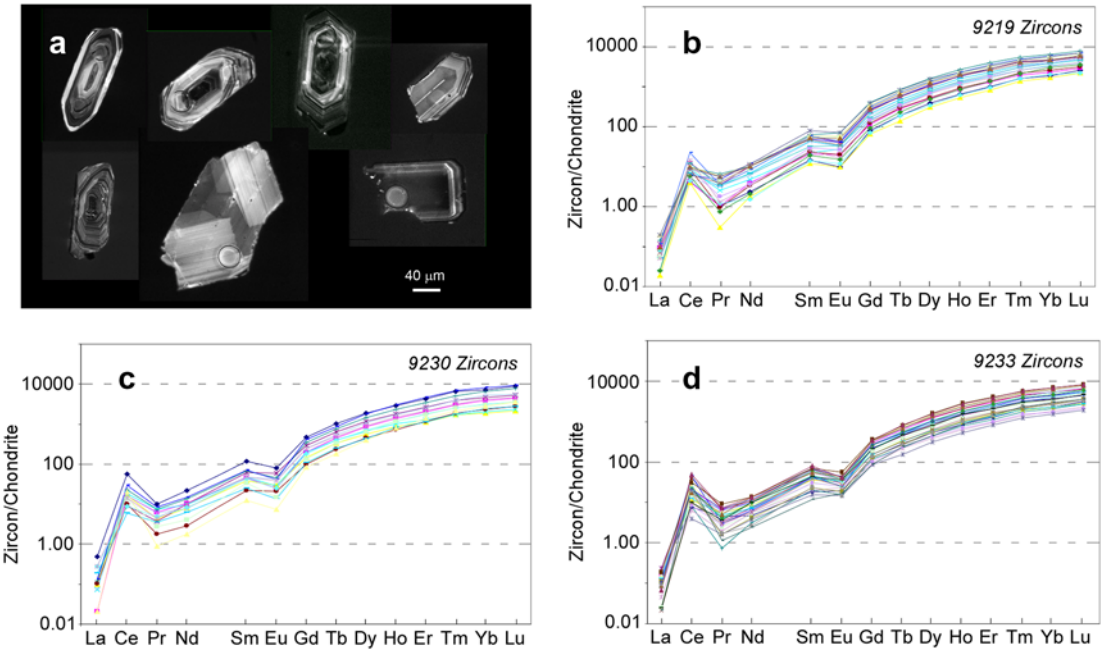

Fig. 9. a Cathodoluminescence (CL) images of the dated zircons (a), and rare earth element patterns of dated zircons in samples 9219, 9230, and 9233 (b, c and d).

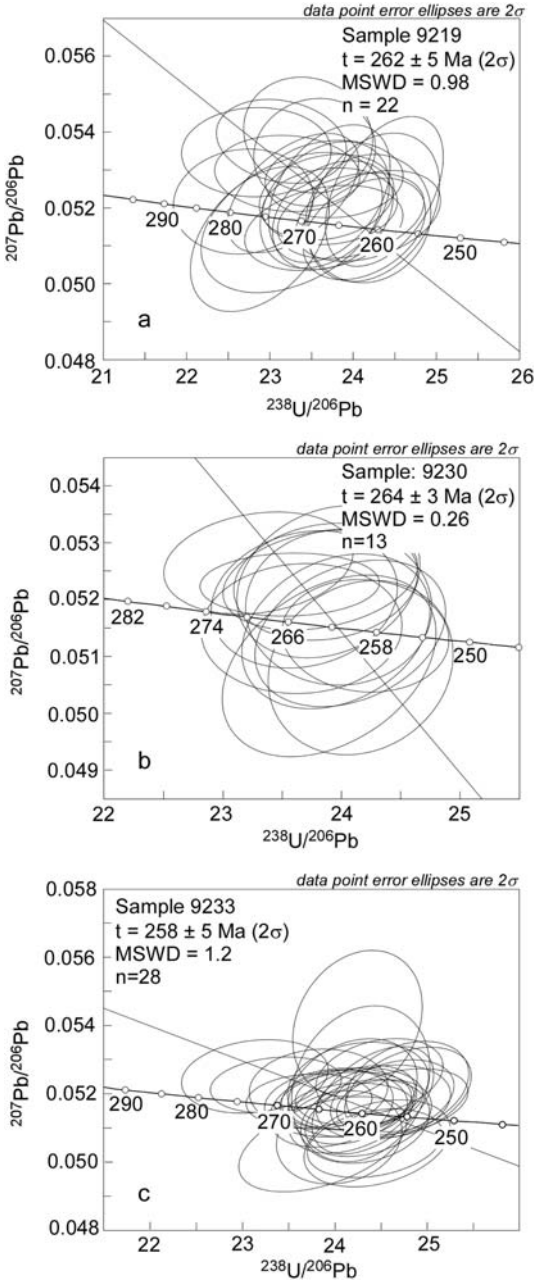

Fig. 10. U-Pb concordia diagrams of zircon ages. a 9219, b 9230 and c 9233. Error ellipses are given at 2σ level. Intercept ages are calculated by Isoplot 3.50 (Ludwig, 2003).

geochemical features of zircons, and (ii) high blocking temperature of zircon (≥900 °C) (e.g., Cherniak and Watson, 2000), the middle Permian ages are interpreted as the age of igneous crystallisation.

7.2. Ar-Ar dating

Dated phengites were separated from a calcschist (7750), a metachert (7751) and a calcite-bearing blueschist (7755B), taken from different domains of the Yenişehir metamorphic rocks along a length of ~60 km (Fig. 2). The samples 7751 and 7755B occur ca. 1–2 km away from the metaophiolitic slice. All of the samples are medium-grained, well-foliated and devoid of any relict texture. The calcschist sample (7750) comprises phengite, chlorite, calcite, epidote, albite, and minor quartz, tourmaline and titanite (Fig. 5d), and secondary minerals such as kaolinite and hematite. Kaolinite and hematite are mostly intergrown with phengite. The metachert sample contains quartz, phengite and tiny grains of garnet (≤20 μm), and minor titanite and rutile (Fig. 5e). Secondary phases are kaolinite and hematite. The blueschist sample (7755B) comprises glaucophane, epidote, phengite, chlorite, albite, and minor titanite and calcite (Fig. 5f). Phengites in all the samples are characterised by Si contents of 3.32–3.50 cations per 11 oxygen anions.

Phengite separates from sample 7750 yielded a steadily increasing, thermally disturbed age spectra with the oldest age value of 202 ± 2 Ma (9th step, 2σ) (Fig. 11a), suggesting loss of radiogenic argon probably due to hydrothermal overprint. Thus, this age is regarded as the minimum age of metamorphism. Presence of kaolinite and hematite locally intergrown with phengite is in line with this interpretation. Sample 7751 records a hump-shaped age spectrum, characterised by steadily increasing age spectra up to the 10th step with an age of 194 ± 3 Ma (2σ), and a decrease in age in the last steps (Fig. 11b), ascribed to the recoil effect which is an artifact of the ^{40}Ar-^{39}Ar technique. It is produced by the recoil of argon from chlorite interlayering during the irradiation (Di Vincenco et al., 2003). Phengite separate from sample 7755B records plateau and integrated latest Triassic age values which are indistinguishable within the range of error ($t_p = 201 \pm 2$ and $t_{int} = 200 \pm 3$ Ma, 2σ, resp.) (Fig. 11c). This age value is within uncertainties indistinguishable from that of the highest age value (9th step) in sample 7750.

To sum up, a latest Triassic age of 201 ± 2 Ma (2σ) can be regarded as geologically meaningful, and interpreted as the timing of greenschist- to blueschist-facies metamorphism, because the dissolution rate of white mica is much faster than the rate of the Fickian diffusion of Ar (Villa, 2015).

8. Discussion

8.1. Age of the accretion and metamorphism

In long-lived subduction complexes, accretion and high-pressure metamorphism take place over an extended period of time. A good example for this is the Franciscan Complex which formed during a period of ca. 150 Ma of subduction, and the blueschist- and higher-grade rocks span an age from ca. 80 to 170 Ma (Wakabayashi, 2015). On the other hand, the age data from the Yenişehir metamorphic rocks, and the relatively uniform grade of metamorphism suggest that the Yenişehir metamorphic rocks including the Boğazköy metaophiolite were accreted and metamorphosed during latest Triassic (201 ± 2 Ma, 2σ). This closely agrees with the Ar-Ar ages of blueschist- and eclogite-facies rocks in Bandırma, ~60 km to the NW, and Eskişehir, ~50 km to the east of the Yenişehir metamorphic rocks (Okay et al., 2002; Okay and Monié, 1997) (Fig. 1).

8.2. Geodynamic implications

The Boğazköy serpentinite represents the mantle section of a former oceanic lithosphere with gabbroic injections, but did it form as a section of a suprasubduction-zone oceanic lithosphere or as a mid-ocean ridge-type oceanic lithosphere? As stated above, the serpentinites were derived from a refractory harzburgite to dunite with roughly U-shaped concave rare earth element patterns. The Cr/(Cr + Al) ratios of the relict Cr-Al spinels (0.45–0.56) in serpentinite are not diagnostic (Fig. 6a). The U-shaped concave rare earth element patterns, with local positive Eu anomalies, however, are documented from several ophiolite complexes such as Oman, Luobusa, and Miaowan (Deng et al., 2017; Godard et al., 2000; Zhou et al., 2005), accounted for by refertilisation of depleted peridotites by LREE enriched melts from suprasubduction-zone setting. Our main argument for their formation in a fore-arc suprasubduction-zone setting come from the wide age span (Middle Devonian to Early Triassic) of the deep sea sedimentary blocks in the Upper Karakaya Complex (Okay et al., 2011, and references therein). Thus, the Permo-Triassic accretionary complexes are products of a long-lived large oceanic domain, rather than a short-lived back-arc setting, and the

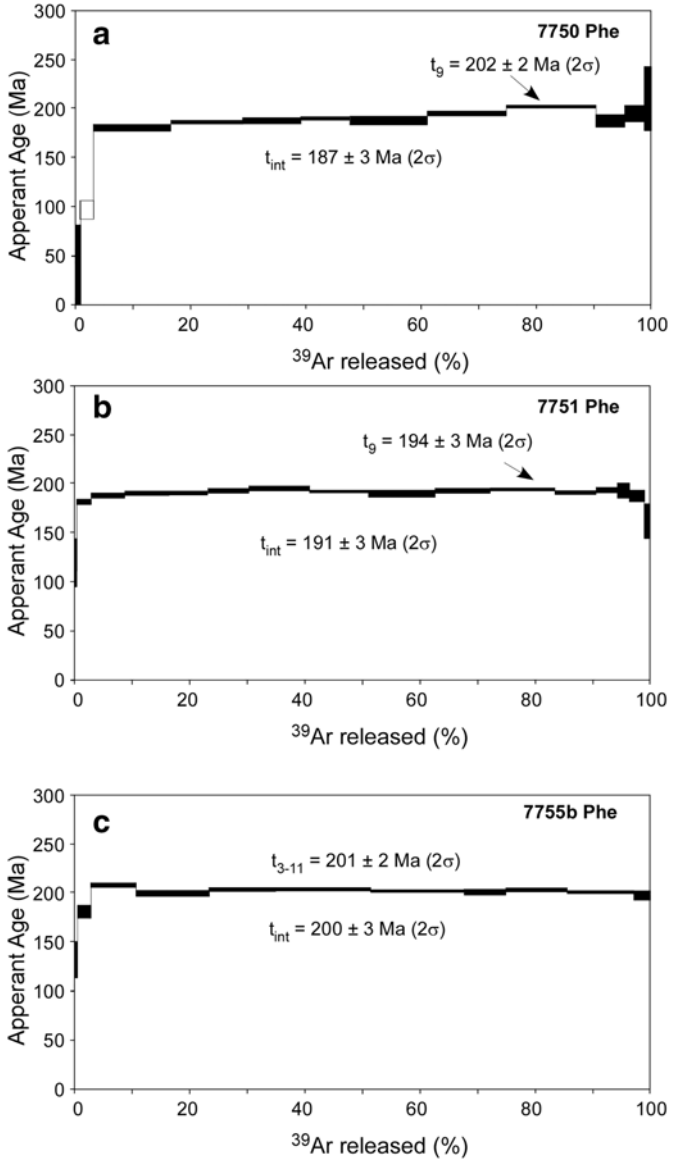

Fig. 11. ^{40}Ar-^{39}Ar release spectra of phengite fractions from dated samples (a 7750, b 7751, and c 7755b) from the Yenişehir metamorphic rocks. See text ('7.2 Ar-Ar dating') for further explanation.

Boğazköy metaophiolite formed during or close to subduction initiation in an oceanic domain dating back at least to Middle Devonian. This interpretation is also consistent with the fact that the oldest accreted and metamorphosed part of the Permo-Triassic accretionary complexes is of middle Permian age (ca. 260 Ma) (Topuz et al., 2004).

There are only three reports on Permian ophiolites in the Tethyan realm: (1) Lesbos island (Greece) (see a in Fig. 1; Koglin et al., 2009), (2) the Almacık mountain (Bolu, Turkey) (see b in Fig. 1; Bozkurt et al., 2013), and (3) the Anarak–Jandaq area in Central Iran (Bagheri and Stampfli, 2008). In a tectonic mélange from the Lesbos island, ~250 km to west of the Yenişehir area, and generally regarded as equivalent of the Karakaya Complex (Fig. 1), a gabbro block with U-Pb zircon age of 253 ± 6 Ma (2σ) has been reported. However, these gabbros were interpreted to have formed in an intracontinental rift-setting (Koglin et al., 2009). In the Almacık Mountain (Bolu, Turkey), a tectonic block, 5 × 15 km, consists of upper amphibolite-facies ultramafic to mafic rock types. The U-Pb zircons from a metaplagiogranite yielded igneous crystallisation ages of 255 ± 2 Ma. However, this unit was interpreted as parts of subcontinental lithospheric mantle, even though the mafic rocks display suprasubduction-zone affinities (Bozkurt et al., 2013). In the Anarak–Jandaq area in Central Iran, Bagheri and Stampfli (2008) describe a metatrondhjemite with U-P zircon age of 262 Ma from a Permian high-pressure metamorphic area. The Boğazköy metaophiolite fragment and aforementioned literature suggest that middle Permian suprasubduction-zone ophiolites may be more common in the Eastern Mediterranean region. The middle Permian probably represents another pulse of suprasubduction-zone ophiolite formation in the Tethyan belt in addition to Early to Middle Jurassic and Late Cretaceous ones.

A question still remains as to how the middle Permian suprasubduction-zone ophiolite was detached from the overriding plate, incorporated accretionary complex and involved in the subduction zone metamorphism during latest Triassic (Fig. 12). Slices or blocks of suprasubduction-zone ophiolites are commonly documented in metamorphic or non-metamorphic accretionary complexes (e.g. MacPherson et al., 1990; Martinez et al., 2007; Zagorevski et al.,

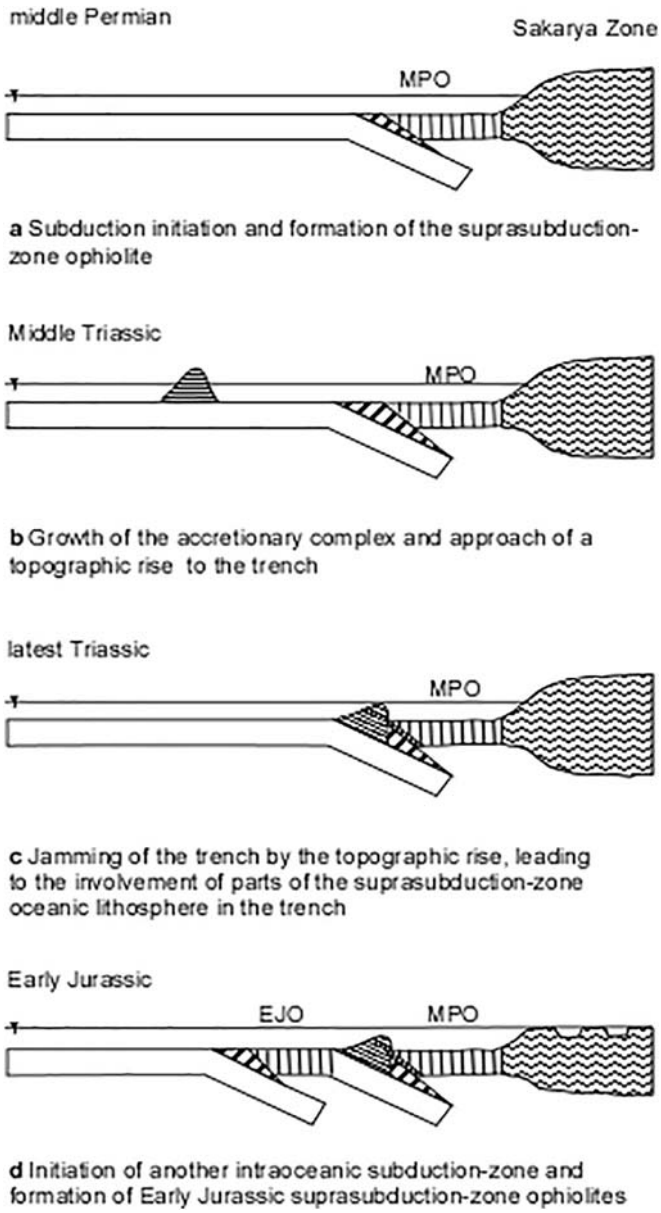

Fig. 12. Schematic illustration of (a) formation of suprasubduction-zone ophiolite during middle Permian (MPO), b growth of the accretionary complex and approach of a topographic rise to the trench, c jamming of the trench by the topographic rise, leading to the involvement of parts of the suprasubduction-zone oceanic lithosphere in the trench, and d initiation of another intraoceanic subduction zone and formation of Early Jurassic suprasubduction-zone ophiolites (EJO).

2009; Wakabayashi et al., 2010; Çelik et al., 2013; Dönmez et al., 2014). Two different mechanisms and their modifications have generally been suggested for their accretion: (i) presence of two coeval intraoceanic subduction-zones in the same oceanic domain, with formation of the suprasubduction-zone ophiolite over one subduction zone, and then subduction and accretion in the another (e.g. Zagorevski et al., 2009; Wakabayashi et al., 2010; Utsunomiya et al., 2011), and (ii) transportation of parts of the suprasubduction-zone ophiolite as olistoliths into the accretionary complex (e.g. MacPherson et al., 1990). We rule out the derivation of the Boğazköy metaophiolite as olistoliths on the basis of its elongated form. We prefer only one intraoceanic subduction-zone rather than two coeval intraoceanic subduction zones, because the Early Jurassic represents the time of the formation of another pulse of suprasubduction-zone ophiolite along southern margin of the Sakarya Zone (e.g. Dilek and Thy, 2006; Rolland et al., 2009; Topuz et al., 2013a, 2013b; Çelik et al., 2013; Göncüoğlu et al., 2012; Robertson et al., 2013) and metabasic rocks in the Late Triassic accretionary complexes display intraplate tholeiitic to alkaline signatures, similar to those in seamounts and oceanic plateaus (e.g. Genç, 2004; Pickett and Robertson, 1996; Sayit et al., 2010). Seeing that suprasubduction-zone ophiolites only form during the initial stages of subduction or somewhat later, and ongoing subduction along the same subduction zone leads either to the growth of the accretionary complex or subduction erosion, the formation of the Early Jurassic suprasubduction-zone ophiolites requires jamming of the Permo-Triassic subduction zone and initiation of another intraoceanic subduction zone. Due to the pull force of the subducting oceanic plate caused by the eclogitisation, stopping of the active subduction zone requires accretion of large topographic highs such as a seamount chain, intraoceanic arc, oceanic plateau or continental fragment. Such a topographic rise is probably an efficient way of detaching parts of the overriding oceanic lithosphere and incorporating it into subduction zone (Fig. 12). Buoyancy analysis indicates that only Hawaii-sized (>8 km-tall?) seamounts and basaltic oceanic plateaus with thicknesses above 17 km can jam the subduction zone (e.g., Cloos, 1993).

9. Conclusions

A meta-ophiolite fragment comprising serpentinite and minor dykes or stocks of metagabbro occurs within a Late Triassic transitional greenschist- to blueschist-facies accretionary complex in the Yenişehir area (NW Turkey). The metagabbros were derived from former plagioclase cumulates. The serpentinite probably represents part of mantle section of the former oceanic lithosphere. Bulk compositions of serpentinite and U-Pb dating of igneous zircons from the metagabbros suggest formation at 262 Ma (late Guadalupian, middle Permian) in a suprasubduction-zone setting, probably related to subduction initiation in the Permian Tethys. During the latest Triassic, parts of the suprasubduction-zone ophiolite were detached from the overriding plate and underwent transitional greenschist–blueschist-facies metamorphism, most probably due to accretion of a large topographic rise to the subduction zone. The age of the oceanic domain, however, likely dates back to the Middle Devonian, as inferred from the ages of the deep sea sedimentary rocks in Permo-Triassic accretionary complexes.

Supplementary data to this article can be found online at https://doi.org/10.1016/j.lithos.2017.12.005.

Acknowledgements

This study has been supported with funds from İTÜ BAP (#39066 and #39282), TÜBA member and TÜBA young scientist award programme. We are grateful to Yalçın Ersoy and one anonymous reviewer for their constructive comments, and Andrew Kerr for painstaking editorial handling. Helps of Mutlu Özkan, İrfan Yolcubal during sample preparation and bulk rock analyses, of Emin Çiftçi during X-ray diffraction studies, of Martin Yates during electron microprobe analyses, and of Erkan Aydar, Evren Çubukçu and Lütfiye Akın during the CL imaging of zircons are gratefully acknowledged.

References

Ague, J.J., 2017. Element mobility during regional metamorphism in crustal and subduction zone environments with a focus on the rare earth elements (REE). American Mineralogist 102, 1796–1821.
Altherr, R., Topuz, G., Marschall, H., Zack, H., Ludwig, T., 2004. Evolution of a tourmaline-bearing lawsonite eclogite from the Elekdağ area (Central Pontides, N Turkey): evidence for infiltration of slab-derived B-rich fluids during exhumation. Contributions to Mineralogy and Petrology 148, 409–425.
Angiboust, S., Agard, P., Jolivet, J., Beyssac, O., 2009. The Zermatt-Saas ophiolite: the largest (60-km wide) and deepest (c. 70–80 km) continuous slice of oceanic lithosphere detached from a subduction zone? Terra Nova 21, 171–180.
Azer, M.K., Stern, R.J., 2007. Neoproterozoic (835–720 Ma) serpentinites in the Eastern Desert, Egypt: fragments of forearc mantle. Journal of Geology 115, 457–472.
Bagheri, S., Stampfli, G.M., 2008. The Anarak, Jandaq and Posht-e-Badam metamorphic complexes in central Iran: new geological data, relationships and tectonic implications. Tectonophysics 451, 123–155.
Boynton, W.V., 1984. Cosmochemistry of the rare earth elements: meteorite studies. In: Henderson, P. (Ed.), Rare Earth Element Geochemistry. Elsevier, Amsterdam, pp. 63–114.
Bozkurt, E., Winchester, J.A., Satır, M., Crowley, Q.G., Ottley, C.J., 2013. The Almacık mafic-ultramafic complex: exhumed Sakarya subcrustal mantle adjacent to the •Istanbul Zone, NW Turkey. Geological Magazine 150, 254–282.
Çapkınoğlu, Ş., Bektaş, O., 1998. Karakaya Kompleksi'ne ait Karasenir formasyonu (Amasya) içindeki kireçtaşı olistolitlerinden Erken Devoniyen konodontları. Maden Tetkik ve Arama Enstitüsü Dergisi 120, 159–170.
Catlos, E.J., Huber, K., Shin, T.A., 2013. Geochemistry and geochronology of meta-igneous rocks from the Tokat Massif, north-central Turkey: implications for Tethyan reconstructions. International Journal of Earth Sciences 102, 2175–2198.
Çelik, Ö.F., Delaloye, M., Feraud, G., 2006. Precise ^{40}Ar-^{39}Ar ages from the metamorphic sole rocks of the Tauride Belt ophiolites, southern Turkey: implications for the rapid cooling history. Geological Magazine 143, 213–227.
Çelik, Ö.F., Chiaradia, M., Marzoli, A., Billor, Z., Marschik, R., 2013. The Eldivan ophiolite and volcanic rocks in the İzmir-Ankara-Erzincan suture zone, northern Turkey: geochemistry, whole-rock geochemical and Nd-Sr-Pb isotopic characteristics. Lithos 172–173, 31–46.
Çelik, Ö.F., Chiaradia, M., Marzoli, A., Özkan, M., Billor, Z., Topuz, G., 2016. Jurassic metabasic rocks in the Kızılırmak accretionary complex (Kargı region, Central Pontides, Northern Turkey). Tectonophysics 672, 34–49.
Cherniak, D.J., Watson, E.B., 2000. Pb diffusion in zircon. Chemical Geology 172, 5–24.
Cloos, M., 1993. Lithospheric buoyancy and collisional orogenesis: subduction of oceanic plateaus, continental margins, island arcs, spreading ridges, and seamounts. Geological Society of America Bulletin 105, 715–737.
Cohen, K.M., Finney, S.C., Gibbard, P.L., Fan, J.-X., 2013. The ICS international chronostratigraphic chart. Episodes 36, 199–204.
Deng, H., Peng, S., Polat, A., Kusky, T., Jiang, X., Han, Q., Wang, L., Huang, Y., Wang, J., Zeng, W., Hu, Z., 2017. Neoproterozoic IAT intrusion into mesoproterozoic MOR Miaowan ophiolite, Yangtze craton: evidence for evolving tectonic settings. Precambrian Research 289, 75–94.
Di Vincenco, G., Viti, C., Rocchi, S., 2003. The effect of chlorite interlayering on ^{40}Ar-^{39}Ar biotite dating: an ^{40}Ar-^{39}Ar laser-probe and TEM investigations of variably choritised biotites. Contributions to Mineralogy and Petrology 145, 643–658.
Dick, H.J.B., Bullen, T., 1984. Chromian spinel as a petrogenetic indicator in abyssal and Alpine-type peridotites and spatially associated lavas. Contributions to Mineralogy and Petrology 86, 54–76.
Dilek, Y., Furnes, H., 2011. Ophiolite genesis and global tectonics: geochemical and tectonic fingerprinting of ancient oceanic lithosphere. Geochemical Society of America Bulletin 123, 387–411.
Dilek, Y., Thy, P., 2006. Age and petrogenesis of plagiogranite intrusions in the Ankara mélange, central Turkey. Island Arc 15, 44–57.
Domeier, M., Torsvik, T.H., 2014. Plate tectonics in the late Paleozoic. Geoscience Frontiers 5, 303–350.
Dönmez, C., Keskin, S., Günay, K., Çolakoğlu, A.O., Çiftci, Y., Uysal, İ., Türkel, A., Yıldırım, N., 2014. Chromite and PGE geochemistry of the Elekdağ ophiolite (Kastamonu, Northern Turkey): implications for deep magmatic processes in a supra-subduction zone setting. Ore Geology Reviews 57, 216–228.
Eyüboğlu, Y., Santosh, M., Bektaş, O., Chung, S., 2011. Late Triassic subduction-related ultramafic-mafic magmatism in the Amasya region (eastern Pontides, N Turkey): implications for the ophiolite conundrum in eastern Mediterranean. Journal of Asian Earth Science 42, 234–257.
Federici, I., Cavazza, W., Okay, A.I., Beyssac, O., Zattin, M., Corrado, S., Dellisanti, F., 2010. Thermal evolution of the Permo-Triassic Karakaya subduction-accretion complex from the Biga Peninsula to the Tokat Massif (Anatolia). Turkish Journal of Earth Sciences 19, 409–429.
Fryer, P., Lockwood, J.P., Becker, N., Phipps, S., Todd, C.S., 2000. Significance of serpentinite mud volcanism in convergent margins. In: Dilek, Y., Moores, E.M., Elthon, D., Nicolas, A. (Eds.), Ophiolites and Oceanic Crust: New Insights from Field Studies and the Ocean Drilling Program: Boulder, Colorado. Geological Society of America Special Paper vol. 349, pp. 35–51.
Genç, Ş.C., 1993. Geologic and Petrologic Investigation of the Tectonic Units Located Between İznik and İnegöl. (PhD Thesis). Istanbul Teknik Universitesi (522 pp.).

Genç, Ş.C., 2004. A Triassic large igneous province in the Pontides, northern Turkey: geochemical data for its tectonic settings. Journal of Asian Earth Sciences 22, 503–516.
Genç, Ş.C., Yılmaz, Y., 1995. Evolution of the Triassic continental margin, northwest Anatolia. Tectonophysics 243, 193–207.
Ghatak, A., Basu, A.R., Wakabayashi, J., 2012. Elemental mobility in subduction metamorphism: insight from metamorphic rocks of the Franciscan Complex and the Feather River ultramafic belt, California. International Geology Review 54 (6), 654–685.
Godard, M., Jousselin, D., Bodinier, J.L., 2000. Relationships between geochemistry and structure beneath a palaeo-spreading centre: a study of the mantle section in the Oman ophiolite. Earth and Planetary Science Letters 180, 133–148.
Göçmengil, G., Altıntaş, I.E., Topuz, G., Çelik, Ö.F., Özkan, M., 2013. Diverse tectonic settings of formation of the metaigneous rocks in the Jurassic metamorphic accretionary complexes (Refahiye, NE Turkey) and their geodynamic implications. Geodinamica Acta 26, 294–310.
Göncüoğlu, M.C., Kuwahara, K., Tekin, U.K., Turhan, N., 2004. Upper Permian (Changxingian) radiolarian cherts within the clastic successions of the "Karakaya Complex" in NW Anatolia. Turkish Journal of Earth Sciences 13, 201–213.
Göncüoğlu, M.C., Marroni, M., Sayit, K., Tekin, U.K., Ottria, G., Pandolfi, L., Ellero, A., 2012. The Aylı Dağ ophiolite sequence (Central Northern Turkey): a fragment of Middle Jurassic oceanic lithosphere within the Intra-Pontide suture zone. Ofioliti 37, 77–92.
Grimes, C.B., John, B.E., Kelemen, P.B., Mazdab, F.K., Wooden, J.L., Cheadle, M.J., Hanghoj, K., Schwartz, J.J., 2007. Trace element geochemistry of zircons from oceanic crust: a method for distinguishing detrital zircon provenance. Geology 35, 643–646.
Hinton, R.W., Upton, B.G.J., 1991. The chemistry of zircon: variations within and between large crystals from syenite and alkali basalts xenoliths. Geochimica et Cosmochimica Acta 55, 3287–3302.
Hoskin, P.W.O., 2005. Trace-element composition of hydrothermal zircon and the alteration of Hadean zircon from the Jack Hills, Australia. Geochemica et Cosmochimica Acta 69, 637–648.
Hoskin, P.W.O., Schaltegger, U., 2003. The composition of zircon and igneous and metamorphic petrogenesis. Reviews in Mineralogy and Geochemistry 53, 27–62.
Huang, Y., Wang, L., Kusky, T., Robinson, P.T., Peng, S., Polat, A., Deng, H., 2017. High-Cr chromites from the late Proterozoic Miaowan Ophiolite Complex, South China: implications for its tectonic environment of formation. Lithos 288–289, 35–54.
Ichiyama, Y., Ishiwatari, A., Kimura, J.-I., Senda, R., Miyamoto, T., 2014. The plume-origin ophiolites in Japan: accreted fragments of oceanic plateaus. Contributions to Mineralogy and Petrology 168, 1–24.
Ishizuka, O., Tani, K., Reagan, M.K., 2014. Izu-Bonin-Mariana forearc crust as a modern ophiolite analogue. Elements 10, 115–120.
Kaczmarek, M.-A., Muntener, O., Rubatto, D., 2008. Trace element chemistry and U–Pb dating of zircons from oceanic gabbros and their relationship with whole rock composition (Lanzo, Italian Alps). Contributions to Mineralogy and Petrology 155, 295–312.
Karaoğlan, F., Parlak, O., Klötzli, U., Thöni, M., Koller, F., 2013. U-Pb and Sm-Nd geochronology of the Kizildag (Hatay, Turkey) ophiolite: implications for the timing and duration of suprasubduction-zone type oceanic crust formation in the southern Neotethys. Geological Magazine 150, 283–299.
Koglin, N., Kostopoulos, D., Reischmann, T., 2009. The Lesbos mafic–ultramafic complex, Greece. Ophiolite or incipient rift? Lithos 108, 243–261.
Kozur, H., Kaya, O., 1994. First evidence of pelagic Late Permian conodonts from NW Turkey. Neues Jahrbuch für Geologie und Paläontologie Monatshefte 6, 339–347.
Kylander-Clark, A.R.C., Hacker, B.R., Cottle, J.M., 2013. Laser-ablation split-stream ICP petrochronology. Chemical Geology 345, 99–112.
Ludwig, K.R., 2003. Isoplot 3.00. A Geochronological Toolkit for Microsoft Excel. Berkeley Geochronology Center Special Publication 4.
MacPherson, G.J., Phipps, S.P., Grossman, J.N., 1990. Diverse sources for igneous blocks in Franciscan melanges, California Coast Ranges. The Journal of Geology 98, 845–862.
Martinez, S.S., Arenas, R., Garcia, F.D., Catalan, J.R.M., Gómez-Barreiro, J., Pearce, J.A., 2007. Careón ophiolite, NW Spain: suprasubduction zone setting for the youngest Rheic Ocean floor. Geology 35, 53–56.
Okay, A.I., 2000. Was the Late Triassic orogeny in Turkey caused by the collision of an oceanic plateau? In: Bozkurt, E., Winchester, J.A., Piper, J.D.A. (Eds.), Tectonic and Magmatism in Turkey and Surrounding Area. Geological Society of London, Special Publication vol. 173, pp. 25–41
Okay, A.I., Göncüoğlu, M.C., 2004. Karakaya Complex: a review of data and concepts. Turkish Journal of Earth Sciences 13, 77–95.
Okay, A.I., Monié, P., 1997. Early Mesozoic subduction in the Eastern Mediterranean: evidence from Triassic eclogite in northwest Turkey. Geology 25, 595–598.
Okay, A.I., Mostler, H., 1994. Carboniferous and Permian radiolarite blocks in the Karakaya Complex in Northwest Turkey. Turkish Journal of Earth Sciences 3, 23–28.
Okay, A.I., Nikishin, A., 2015. Tectonic evolution of the southern margin of Laurasia in the Black Sea region. International Geology Review 57, 1051–1076.
Okay, A.I., Topuz, G., 2017. Variscan orogeny in the Black Sea region. International Journal of Earth Sciences 106, 569–592.
Okay, A.I., Monod, O., Monié, P., 2002. Triassic blueschists and eclogites from northwest Turkey: vestiges of the Paleo-Tethyan subduction. Lithos 64, 155–178.
Okay, A.I., Satır, M., Zattin, M., Cavazza, W., Topuz, G., 2008. An Oligocene ductile strike-slip shear zone: the Uludağ Massif, northwest Turkey-implications for the westward translation of Anatolia. Geological Society of America Bulletin 120, 893–911.
Okay, A.I., Noble, P.J., Tekin, U.K., 2011. Devonian radiolarian ribbon cherts from the Karakaya Complex, NW Turkey: implications for the Paleo-Tethyan evolution. Comptes Rendus Palevol 10, 1–10.
Parlak, O., Delaloye, M., 1999. Precise ^{40}Ar–^{39}Ar ages from the metamorphic sole of the Mersin ophiolite (Southern Turkey). Tectonophysics 301, 145–158.
Paton, C., Hellstrom, J., Paul, B., Woodhead, J., Hergt, J., 2011. Iolite: freeware for the visualization and processing of mass spectrometric data. Journal of Analytical Atomic Spectrometry 26, 2508–2518.
Pearce, J.A., 2003. Supra-subduction zone ophiolites: the search for modern analogues. In: Dilek, Y., Newcomb, S. (Eds.), Ophiolite Concept and the Evolution of Geological Thought. Geological Society of America, Boulder, Colorado, Special Paper 373, pp. 269–294.
Pearce, J.A., 2014. Immobile element fingerprinting of ophiolites. Elements 10, 101–108.
Pearce, J.A., Robinson, P.T., 2010. The Trodos ophiolitic complex probably formed in a subduction initiation, slab edge setting. Gondwana Research 18, 60–81.
Pickett, E.A., Robertson, A.H.F., 1996. Formation of the Late Paleozoic-Early Mesozoic Karakaya Complex and related ophiolites in NW Turkey by Paleotethyan subduction-accretion. Journal of the Geological Society, London 153, 995–1009.
Polat, A., Hofmann, A.W., 2003. Alteration and geochemical patterns in the 3.7–3.8 Ga Isua greenstone belt, West Greenland. Precambrian Research 126, 197–218.
Renne, P.R., Mundil, R., Balco, G., Min, K., Ludwig, K.R., 2010. Joint determination of ^{40}K decay constants and $^{40}Ar/^{40}K$ for the Fish Canyon sanidine standard, and improved accuracy for $^{40}Ar/^{39}Ar$ geochronology. Geochimica et Cosmochimica Acta 74, 5349–5367.
Renne, P.R., Balco, G., Ludwıg, K.R., Mundil, R., Min, K., 2011. Response to the comment by W.H. Schwarz et al. on "Joint determination of ^{40}K decay constants and $^{40}Ar/^{40}K$ for the Fish Canyon sanidine standard, and improved accuracy for $^{40}Ar/^{39}Ar$ geochronology" by P.R. Renne et al. (2010). Geochimica et Cosmochimica Acta 75, 5097–5100.
Robertson, A.H.F., Ustaömer, T., 2012. Testing alternative tectono-stratigraphic interpretations of the Late Palaeozoic–Early Mesozoic Karakaya complex in NW Turkey: support for an accretionary origin related to northward subduction of Palaeotethys. Turkish Journal of Earth Sciences 21, 961–1007.
Robertson, A.H.F., Parlak, O., Ustaomer, T., Tasli, K., Inan, N., Dumitrica, P., Karaoğlan, F., 2013. Subduction, ophiolite genesis and collision history of Tethys adjacent to the Eurasian continental margin: New evidence from the Eastern Pontides, Turkey. Geodinamica Acta 26, 230–293.
Rolland, Y., Galoyan, Gh., Bosch, D., Sosson, M., Corsini, M., Fornari, M., Vérati, C., 2009. Jurassic back-arc and hot-spot related series in the Armenian ophiolites – implications for the obduction process. Lithos 112, 163–187.
Saumur, B.-M., Hattori, K.H., Guillot, S., 2010. Contrasting origins of serpentinites in a subduction complex, northern Dominican Republic. Geological Society of America Bulletin 122, 292–304.
Sayit, K., Göncüoğlu, M.C., Furman, T., 2010. Petrological reconstruction of Triassic seamounts/oceanic islands within Palaeotethys: geochemical implications from the Karakaya subduction/accretion complex, Northern Turkey. Lithos 119, 501–511.
Schwarz, W.H., Trieloff, M., 2007. Intercalibration of ^{40}Ar-^{39}Ar age standards NL25, HB3gr hornblendes, GA-1550, SB-3, HD-B1 biotite and Bmus/2 muscovite. Chemical Geology 241, 218–231.
Schwarz, W.H., Kossert, K., Trieloff, M., Hopp, J., 2011. Comment on the "Joint determination of ^{40}K decay constants and $^{40}Ar/^{40}K$ for the Fish Canyon sanidine standard, and improved accuracy for $^{40}Ar/^{39}Ar$ geochronology" by Paul R. Renne et al. (2010). Geochimica et Cosmochimica Acta 75, 5094–5096.
Schwarz, W.H., Henke, S., Trieloff, M., Gail, H.-P., 2012. Revision of the K decay constants. 34th IGC in Brisbane, p. 3139.
Şengör, A.M.C., 1984. The Cimmeride orogenic system and the tectonics of Eurasia. Geological Society of America Special Paper vol. 195. Geological Society of America, Boulder, CO (82 pp.).
Şengör, A.M.C., Atayman, S., 2009. The Permian extinction and the Tethys: an exercise in global geology. Geological Society of America, Special Paper 448, 85.
Shervais, J.W., 2001. Birth, death, and resurrection: the life cycle of suprasubduction zone ophiolites. Geochemistry, Geophysics, Geosystems 2 (2000GC000080).
Singh, A.K., Singh, R.B., 2013. Genetic implications of Zn- and Mn-rich Cr-spinels in serpentinites of the Tidding Suture Zone, eastern Himalaya, NE India. Geological Journal 48, 22–38.
Stampfli, G.M., Borel, G.D., 2002. A plate tectonic model for the Paleozoic and Mesozoic constrained by dynamic plate boundaries and restored synthetic oceanic isochrones. Earth and Planetary Science Letters 196, 17–33.
Steiger, R.H., Jäger, E., 1977. Subcommission on geochronology: convention on the use of decay constants in geo- and cosmochronology. Earth and Planetary Science Letters 36, 359–362.
Stern, R.J., Bloomer, S.H., 1992. Subduction zone infancy: examples from the Eocene Izu-Bonin-Mariana and Jurassic California arcs. Geological Society of America Bulletin 104, 1621–1636.
Tekeli, O., 1981. Subduction complex of pre-Jurassic age, northern Anatolia, Turkey. Geology 9, 68–72.
Topuz, G., Okay, A.I., 2017. Late Eocene–Early Oligocene two-mica granites in NW Turkey (the Uludağ Massif): water-fluxed melting products of a mafic metagreywacke. Lithos 268–271, 334–350.
Topuz, G., Altherr, R., Satır, M., Schwarz, M., 2004. Low grade metamorphic rocks from the Pulur complex, NE Turkey: implications for pre-Liassic evolution of the Eastern Pontides. International Journal of Earth Sciences 93, 72–91.
Topuz, G., Okay, A.I., Altherr, R., Satır, M., Schwarz, W.H., 2008. Late Cretaceous blueschist-facies metamorphism in southeastern Thrace (Turkey) and its geodynamic implications. Journal of Metamorphic Geology 26, 895–913.
Topuz, G., Göçmengil, G., Rolland, Y., Çelik, Ö.F., Zack, T., Schmitt, A.K., 2013a. Jurassic accretionary complex and ophiolite from northeast Turkey: no evidence for the Cimmerian continental ribbon. Geology 45, 255–258.
Topuz, G., Çelik, Ö.F., Şengör, A.M.C., Altıntaş, İ.E., Zack, T., Rolland, Y., Barth, M., 2013b. Jurassic ophiolite formation and emplacement as backstop to a subduction-accretion complex in northeast Turkey, the Refahiye ophiolite, and relation to the Balkan ophiolites. American Journal of Science 313, 1054–1087.
Topuz, G., Okay, A.I., Altherr, R., Schwarz, W.H., Sunal, G., Altınkaynak, L., 2014. Triassic warm subduction in northeast Turkey: evidence from the Ağvanis metamorphic rocks. Island Arc 23, 181–205.

Türkecan, A., Yurtsever, A., 2002. Geological map of Turkey, Istanbul sheet, 1:500000. Maden Tetkik ve Arama Ernstitüsü Genel Müdürlüğü (MTA), Ankara, Turkey.
Ustaömer, T., Ustaömer, P.A., Robertson, A.H.F., Gerdes, A., 2016. Implications of U-Pb and Lu-Hf isotopic analysis of detrital zircons for the depositional age, provenance and tectonic setting of the Permian-Triassic Palaeotethyan Karakaya Complex, NW Turkey. International Journal of Earth Sciences 105, 7–38.
Utsunomiya, A., Jahn, B.-M., Okamoto, K., Ota, T., Shinjoe, H., 2011. Intra-oceanic island arc origin for Iratsu eclogites of the Sanbagawa belt, central Shikoku, southwest Japan. Chemical Geology 280, 97–114.
van Hinsbergen, D.J.J., Maffione, M., Plunder, A., Kaymakçi, N., Ganerød, M., Hendriks, B.W.H., Corfu, F., Gürer, D., de Gelder, G.I.N.O., Peters, K., McPhee, P.J., Brouwer, F.M., Advokaat, E.L., Vissers, R.L.M., 2016. Tectonic evolution and paleogeography of the Kırşehir Block and the Central Anatolian Ophiolites, Turkey. Tectonics 35, 983–1014.
Villa, I.M., 2015. ^{39}Ar-^{40}Ar geochronology of mono- and polymetamorphic basement rocks. Periodico di Mineralogia 84, 615–632.
Wakabayashi, J., 2012. Subducted sedimentary serpentinite mélanges: record of multiple burial-exhumation cycles and subduction erosion. Tectonophysics 568–569, 230–247.
Wakabayashi, J., 2015. Anatomy of a subduction complex: architecture of the Franciscan Complex, California, at multiple length and time scales. International Geology Review 57, 669–746.
Wakabayashi, J., 2017. Serpentinites and serpentinites: variety of origins and emplacement mechanisms of serpentinite bodies in the California Cordillera. Island Arc. https://doi.org/10.1111/iar.12205.
Wakabayashi, J., Ghatak, A., Basu, A.R., 2010. Suprasubduction-zone ophiolite generation, emplacement, and initiation of subduction: a perspective from geochemistry, metamorphism, geochronology, and regional geology. Geological Society of America Bulletin 122, 1548–1568.
Warren, C.J., Parrish, R.R., Waters, D.J., Searle, M.P., 2005. Dating the geologic history of Oman's Semail ophiolite: insights from U-Pb geochronology. Contributions to Mineralogy and Petrology 150, 403–422.
Yılmaz, A., Yılmaz, H., 2004. Geology and structural evolution of the Tokat Massif (Eastern Pontides, Turkey). Turkish Journal of Earth Sciences 13, 231–246.
Yılmaz, Y., Serdar, H.S., Genç, C., Yiğitbaş, E., Gürer, Ö.F., Elmas, A., Yıldırım, M., Bozcu, M., Gürpınar, O., 1997. The geology and evolution of the Tokat Massif, South-Central Pontides, Turkey. International Geological Review 39, 365–382.
Zagorevski, A., Lissenberg, C.J., van Staal, C.R., 2009. Dynamics of accretion of arc and backarc crust to continental margins: inferences from the Annieopsquotch accretionary tract, Newfoundland Appalachians. Tectonophysics 479, 150–164.
Zhou, M.F., Robinson, P.T., Malpas, J., Edwards, S.J., Qi, L., 2005. REE and PGE geochemical constraints on the formation of dunites in the Luobusa ophiolite, Southern Tibet. Journal of Petrology 46, 615–639.